

# Molten Metals and Molten Carbonates in Solid Oxide Direct Carbon Fuel Cell Anode Chamber: Liquid Metal Anode and Hybrid Direct Carbon Fuel Cells

Ermete Antolini

Scuola di Scienza dei Materiali, Via 25 Aprile 22, 16016 Genova, Italy; ermantol@libero.it

**Abstract:** To enhance the contact between the electrolyte (source of  $O^{2-}$ ) and the carbon fuel in solid oxide–direct carbon fuel cells (SO-DCFCs), molten metals and molten salts were used in the anode chamber. Oxygen ions can dissolve and be transported in the molten medium to the anode three-phase boundary to reach and oxidize the carbon particles. To improve the sluggish kinetics of the electrochemical oxidation of carbon, the same molten media can act as redox mediators. Moreover, using a liquid metal/salt anode, tolerant to fuel impurities, the negative effect of carbon contaminants on cell performance is mitigated. In this work, an overview of SO-DCFCs with liquid metals, liquid carbonates, and mixed liquid metals/liquid carbonates in the anode chamber is presented and their performance was compared to that of conventional SO-DCFCs.

**Keywords:** solid oxide fuel cell; direct carbon fuel cell; molten anode; molten carbonates

## 1. Introduction

Direct carbon fuel cells (DCFCs) have attracted growing interest as a power generation device that directly converts the chemical energy of solid carbon, a low-cost widely available fuel, to electrical energy [1,2]. DCFCs have a theoretical 100% electrochemical efficiency of converting chemical energy to electricity, more than twice that from thermal conversion [3,4], giving an actual efficiency of around 80%, higher than that of molten carbonate fuel cells (MCFCs) or solid oxide fuel cells (SOFCs), fueled with hydrogen or natural gas (45–60%) [3]. Similar to other fuel cells, a DCFC is formed by an anode, a cathode, an electrolyte, and a current collector. The main difference is the use of a solid fuel. Generally, DCFCs can be classified as molten hydroxide (MH-DCFCs), molten carbonate (MC-DCFCs), or solid oxide direct carbon fuel cells (SO-DCFCs), depending on the type of electrolyte [3,4]. Among them, SO-DCFCs are the most investigated. SOFCs have a number of advantages compared to the other types of fuel cells, due to their solid materials and high operating temperature. Since all the components are solid, there is no electrolyte loss, and electrode corrosion is eliminated. As SOFCs are operated at high temperature, there is no need to use expensive catalysts such as platinum or palladium. Moreover, because of high-temperature operation, another advantage of SOFC over other types of fuel cell is its tolerance to the impurities of inlet fuels, meaning that various types of fuel can be applied with SOFC. Due to high-quality waste heat for cogeneration applications and low activation losses, they have a great efficiency for electricity production. There are also some disadvantages due to the high operating temperature. The materials used are thermally challenged. The relatively high cost and complex fabrication are also significant problems that need to be solved. The recent advances in SO-DCFCs were reviewed by Yu et al. [5]. In an SO-DCFC, at the cathode side, oxygen is



**Citation:** Antolini, E. Molten Metals and Molten Carbonates in Solid Oxide Direct Carbon Fuel Cell Anode Chamber: Liquid Metal Anode and Hybrid Direct Carbon Fuel Cells. *Catalysts* **2023**, *13*, 1107. <https://doi.org/10.3390/catal13071107>

Academic Editor: Vincenzo Baglio

Received: 10 June 2023

Revised: 10 July 2023

Accepted: 12 July 2023

Published: 15 July 2023



**Copyright:** © 2023 by the author. Licensee MDPI, Basel, Switzerland. This article is an open access article distributed under the terms and conditions of the Creative Commons Attribution (CC BY) license (<https://creativecommons.org/licenses/by/4.0/>).

reduced to oxygen ions; then,  $O^{2-}$  ions are transferred through the electrolyte to the anode three-phase boundary (TPB, the interphase between electrolyte, electrode, and gas/solid chemical species), where they react with carbon to generate  $CO_2$  [2,6]:



The carbon particles in direct contact with the electrolyte can also be electro-oxidized sequentially to CO and  $CO_2$  [7]:



The carbon particles not in direct contact with the electrolyte can be oxidized via the non-electrochemical reverse Boudouard reaction:



Reaction (5) can occur anywhere in the anode chamber and, in the presence of  $CO_2$ , even when the cell is in the open-circuit condition, and does not contribute to the cell voltage. At temperatures above 700 °C, the reverse Boudouard reaction is strongly favored [2].

The use of carbon in SOFCs, however, presents some disadvantages: compared to conventional fuels, carbon is less reactive and is not a fluid, making the interaction between the carbon particles and the solid anode/electrolyte difficult. To improve the contact between the electrolyte and carbon, molten metals/salts were placed in the anode chamber.  $O^{2-}$  can be dissolved and transported in the molten medium to the TPB to reach carbon particles and to complete cell reactions. Molten media can also act as redox mediators, to improve the sluggish kinetics of electrochemical carbon oxidation. Moreover, the degradation of the anode catalyst by carbon contaminants can be mitigated by using a liquid metal/liquid carbonate anode [8,9]. Liquid metals/liquid carbonates were initially used as anode catalysts in the place of solid anode catalysts. Then, overall, molten carbonates and, sometimes, molten metals were utilized together with a solid anode catalyst as facilitators of the electrolyte/anode contact with carbon and as redox mediators. A scheme reporting the various types of liquid metal/liquid carbonate DCFCs is shown in Figure 1. In this work, an overview of SO-DCFCs with liquid metals, liquid carbonates, and mixed liquid metals/liquid carbonates in the anode chamber is presented and their performance was compared to that of conventional SO-DCFCs.

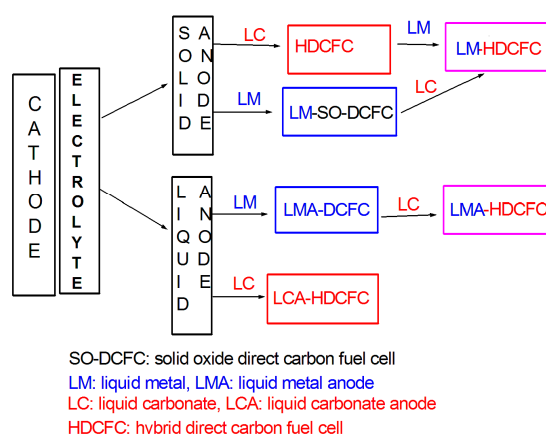


**Figure 1.** A scheme reporting the various types of liquid metal/liquid carbonate direct carbon fuel cells.

## 2. Liquid Metal Anode–Direct Carbon Fuel Cells (LMA-DCFCs)

A schematic configuration of an LMA-DCFC is shown in Figure 2. The arrangement of an LMA-DCFC is the same as that of a conventional SOFC, except that the anode is a liquid metal. The liquid metal anode has a high tolerance to carbon impurities, such as sulfur and NO<sub>x</sub> [10]. Also, the ash can float on the liquid metal surface and can be easily removed. In addition, the liquid anode presents other suitable features: (i) the carbon active area can be effectively increased, by turning the solid electrode/solid carbon into a liquid electrode/solid carbon contact [8,9]; (ii) as the liquid metal is electronically conductive, the electrochemical reaction can be performed at the entire electrolyte/liquid metal interface; (iii) the molten metal, as an energy storage medium, can operate for a short period of time without fuels, in the battery mode, minimizing the negative effect of discontinuous fuel delivery [8]. First, Yentekakis et al. [11,12] reported the gasification of coal with the simultaneous generation of electricity in an SOFC with a molten iron anode, an yttria-stabilized zirconia (YSZ) electrolyte immersed in the molten anode, and a Pt [11] or a perovskite [12] cathode, with carbon particles dispersed in the molten iron. A mathematical model was developed, describing the steady-state behavior of this fuel cell and the effect of operating conditions on cell performance. The electrochemical cell generated very high current and power densities. However, as the SOFC operating temperature has to be higher than the iron melting point (1535 °C), their model was constructed for extremely high temperatures.

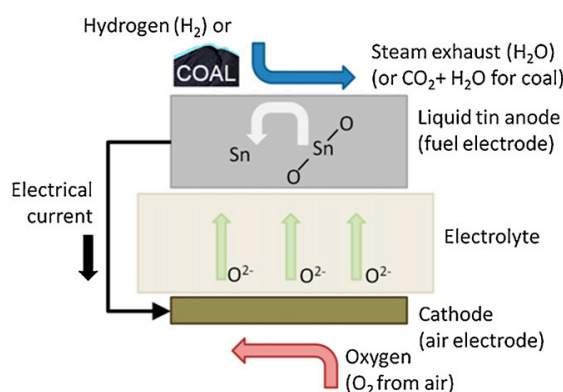
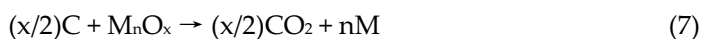


**Figure 2.** Liquid metal anode SOFC, with tin as the metal. Reproduced from Ref. [9], copyright 2011, with permission from Elsevier.

The liquid metal anode can act as a chemical intermediary for the oxidation of fuel. The anodic reaction can be split into two reactions [4,13]:



Metal oxidation (reaction 6) takes place at the liquid anode–electrolyte interface, whereas carbon oxidation and metal reduction (reaction 7) occur at the fuel–anode interface. The reaction between metal oxide and carbon takes place as they are in intimate contact, but the reaction is slow if the oxide is solid at the fuel cell operation temperature, as for SnO<sub>2</sub>. In the case of Sb<sub>2</sub>O<sub>3</sub>, which is liquid at the fuel cell operation temperature, instead, this reaction is fast. Only the first step is electrochemical. The desired reaction, however, is the direct reaction between carbon and dissolved oxygen in the metal. The open-circuit voltage (OCV) for this reaction versus air depends on the type of carbon, but it is near 1 V [8,9]. If the reaction of oxygen is directly with carbon, the conventional OCVs will be held, which are generally higher than those of the reaction with the metal. Indeed, in the 700–1000 °C temperature range, the oxidation potential for spontaneous metal oxidation reaction is less than 1 V, resulting in a significant energy loss. To promote re-

action 2, it is appropriate to use a metal with a low oxygen affinity and a high solubility of fuel and oxygen. Copper and silver fulfill these requirements. Among them, silver is preferred as it has a higher oxygen solubility and lower melting temperature than copper. Ag is also an excellent electronic conductor, with a good wetting ability for YSZ, a common SOFC electrolyte [14]. Moreover, Ag does not form stable oxides at SOFC operating temperatures [14], does not react with carbon, and does not form a carbide phase. Thus, carbon can be dispersed into the molten Ag without degradation [14]. Copper [15] and silver [16] were tested as metal anodes in LMA-DCFCs, but, due to their high melting point, the cell operation temperature was  $\geq 1000$  °C. For its use as a liquid metal anode, the melting temperature of the metal has to be below SOFC operating temperatures (700–1000 °C). Low-melting-point metals, such as tin, indium, bismuth, lead, and antimony, were tested as the anode of an LMA-DCFC [8–10,17–21]. As these metals also act as chemical mediators, their metal oxides have to be reduced by carbon spontaneously. The values of OCV for metal oxidation are in the order  $\text{Sn} > \text{Sb} > \text{Pb} > \text{Bi}$  [8]. Due to the low melting point and the high OCV at 800 °C (0.897 V), only near 0.1 V lower than that for carbon oxidation to  $\text{CO}_2$ , Sn has been given much attention. However, a solid insulating  $\text{SnO}_2$  layer forms at the electrolyte interface during fuel cell operation, inhibiting the further transfer of oxygen from the electrolyte [17]. This drawback is observed using carbon as the fuel, whereas it is less important when using hydrogen [22], as  $\text{H}_2$  can effectively reduce  $\text{SnO}_2$  [23]. Thus, to use carbon as the fuel, besides Sn, other metals were investigated [23]. Bi presents a low resistance because of its ionically conductive oxide, but it has a low OCV. Both Pb and Sb have a low resistance and form oxides having relatively low melting temperatures, 888 °C for  $\text{PbO}$  and 656 °C for  $\text{Sb}_2\text{O}_3$ . This allows the oxides to be removed from the interface between the electrolyte and anode. Among them, Sb is the most promising because of its higher OCV and lower oxide melting temperature.

Preliminary works were carried out on liquid tin anode–direct carbon fuel cells (LTA-DCFCs) [10,24,25]. First, at CellTech, Westborough, MA, USA, the use of a molten tin anode in an SOFC was investigated [10,24]. To avoid the formation of an oxide layer, the LTA-SOFC operates at over 1000 °C, since  $\text{SnO}_2$  formation is thermodynamically unfavorable at this temperature. At EPRI, an LTA-DCFC power plant based on CellTech technology was evaluated and compared with hybrid direct carbon fuel cell (HDCFC) and MC-DCFC power plants [25]. This cell is a tubular-cathode-supported SOFC with a molten tin anode and an YSZ electrolyte layer.  $\text{O}^{2-}$ , formed at the cathode and transferred at the anode through the electrolyte layer, oxidizes Sn to  $\text{SnO}_2$ . Then, a large amount of molten Sn flows with  $\text{SnO}_2$  to the tin bath, where coal reduces  $\text{SnO}_2$  back to Sn. The power density and cell efficiency are  $196 \text{ mW cm}^{-2}$  and 83.85%, respectively. Among the DCFCs investigated, the molten-tin cycle has the lowest efficiency because coal is not fed into the fuel cell stacks directly, but it uses the Sn redox reaction as an intermediate step. Then, starting from 2011, various papers addressed DCFCs with a liquid metal anode. Literature data on liquid metal DCFCs are reported in Table 1 [13,15,16,19,20,22,26–35]. As can be seen in Table 1, only Sn and, in particular, Sb, alone or mixed with another metal, were investigated.

**Table 1.** Literature data on liquid metal DCFCs, including intrinsic parameters (catalysts and electrolyte), operational parameters (fuel type and temperature), maximum power density (MPD), and power density (PD) at a constant current or potential. The results are sorted by increasing year. \* In SbBi, Sb oxidizes, Bi does not.

Molten Metal	Anode//Electrolyte//Cathode	Fuel	T °C	OCV V	MPD mWcm <sup>-2</sup>	PD (mWcm <sup>-2</sup> ) at Constant j (mA cm <sup>-2</sup> ) or V	Ref.
Cu	Cu//YSZ//La <sub>0.9</sub> Sr <sub>0.1</sub> (Mn,Fe,Co)O <sub>3-δ</sub>	Desulfurized coke	1100	1.2	1700		[15]
Sb	Sb//ScSZ//La <sub>0.8</sub> Sr <sub>0.2</sub> FeO <sub>3</sub> (LSF)-ScSZ, Sb 2 g	Sugar char 0.5 g	700	0.75	360	300 (0.5 V) Stable > 12 h	[26]
Sb SbBi *	Sb(Sb <sub>0.8</sub> Bi <sub>0.2</sub> )//ScSZ//La <sub>0.8</sub> Sr <sub>0.2</sub> FeO <sub>3</sub> (LSF)-S cSZ, Sb 10 g, SbBi 13.5 g	60% charcoal 40% rice starch, 13 g, refueling	700	0.75 0.738		ca. 250 (0.5 V) (>200 h)	[13]
Ag Ag <sub>0.5</sub> Sb <sub>0.5</sub>	Ag//YSZ//LSF, Ag 2 g AgSb//YSZ//LSF, Sb 2g	Charcoal, 0.5 g	1000 700	1.12 0.75	≈8 ≈60	-	[16]
Sn	Ni/YSZ//YSZ//La <sub>0.8</sub> Sr <sub>0.2</sub> MnO <sub>3</sub> (LSM)	Carbon black (C <sub>b</sub> )	900	0.68	14		[27]
		Sn + C <sub>b</sub> (Sn:C <sub>b</sub> 1:3)	900	0.71	60.5		
		Sn + Ni + C <sub>b</sub>	900	0.73	105		
Sb	Sb//SmDC//Ba <sub>0.5</sub> Sr <sub>0.5</sub> Co <sub>1-x</sub> Fe <sub>x</sub> O <sub>3-δ</sub> (BSCF)	Carbon	650		222		[28]
			700		268		
			750		327		
Sn	Sn//YSZ//Pt, Sn 2 g Sn//YSZ//Pt after 10 h	Carbon black 0.2 g	800	0.85	≈0.5	-	[22]
			800	0.75	≈1.0		
Sb	Sb//YSZ//Pt, Sb 10 g	De-ash coal, 1 g after discharging	800	0.704	72	66 (0.3 V) Stable > 2 h	[29]
Sb	Sb//YSZ//Pt, Sb 10 g	De-ash coal, 1 g after discharging	900	0.66	≈100	98 (0.3 V)	[20]
		Well-mixed Sb and C (direct carbon oxidation)	800	1.083	≈23	Stable > 1 h	
Sn	Sn//YSZ//LSM	Coal	900	0.885	-		[30]
Sb	Sb//YSZ//La <sub>0.6</sub> Sr <sub>0.4</sub> Co <sub>0.2</sub> Fe <sub>0.8</sub> O <sub>3</sub> -Gd <sub>2</sub> O <sub>3</sub> dop ed CeO <sub>2</sub> (LSCF-10GDC), Sb 5 g	Activated carbon 1 g	800	0.69 (no C)	304 (no C)	200 (400) Stable > 6 h	[19]
Sb	Sb//YSZ//LSCF-10GDC, Sb 5 g	Pyrolyzed cocoonut shells (CAC), SSA 749 m <sup>2</sup> g <sup>-1</sup>	750	0.712 (no C)	196 (no C)	CAC 180 (400), 14 h	[31]
		pyrolyzed fresh corn starch (PCS) SSA 0.2 m <sup>2</sup> g <sup>-1</sup>	800	0.69 (no C)	304 (no C)	PCS 180 (400), 1 h	
		2g				CAC 208 (400), 11 h PCS 208 (400), 11 h	
Sn	Ni/YSZ//YSZ//LSM Sn/Ni/YSZ//YSZ//LSM, Sn 15 mg Sn/Ni/YSZ//YSZ//LSM, Sn 60 mg Ni/YSZ//LSM Sn/Ni/YSZ//YSZ//LSM, Sn 15 mg Sn/Ni7YSZ//YSZ//LSM, Sn 60 mg	Carbon black 0.3 g		0.91	20		[32]
				0.95	62		
			750	0.85	30		
			850	0.88	68		
				0.91	136		
				0.87	95		
Sn	Ni/YSZ//YSZ//GDC/LSCF/GDC	Sn		0.86	59		[33]
		Lignite (PCF)		0.95	77		
		PAC		0.92	74		
		Sn + PCF (Sn:C 4:1)		0.76	51		
		Sn + PAC(Sn:C 4:1)	750	1.0	97		
		Sn	850	0.88	89		
		PCF		1.01	123		
		PAC		0.97	119		
		Sn + PCF (Sn:C 4:1)		0.91	75		
		Sn + PAC(Sn:C 4:1)		1.03	161		
Sb	Sb <sub>1-x</sub> Ag <sub>x</sub> //YSZ//LSCF-10GDC, Sb 5 g	CAC, 2 g		0.71	226		[34]
Sb <sub>0.9</sub> Ag <sub>0.1</sub>				0.74	225		
Sb <sub>0.8</sub> Ag <sub>0.2</sub>			800	0.705	203		
Sb <sub>0.7</sub> Ag <sub>0.3</sub>				0.7	187		
Sb	Sb//Sb <sub>2</sub> O <sub>3</sub> /YSZ//LSM/YSZ	De-ash anthracite coal, 10 g refueling	700	0.745	35	25 (0.35 V)	[35]
			750	0.723	47	Stable > 40 h	

## 2.1. Molten Tin–Direct Carbon Fuel Cells

There are two types of liquid tin DCFCs, the properly said LTA-DCFCs, where molten tin acts as the anode, and liquid-tin-containing SO-DCFCs, where molten tin is added to a typical SOFC, with a solid Ni/YSZ anode.

### 2.1.1. LTA-DCFCs

Only two works addressed LTA-DCFCs, and in both papers, a poor performance was reported [23,30], due to the presence of an insulating  $\text{SnO}_2$  layer. The cell performance in battery mode, gas fuel mode, and solid carbon mode was compared, using a YSZ electrolyte and a Pt [23] or perovskite [30] cathode.

As reported by Wang et al. [23], at 800 °C, in battery mode, the formation of a  $\text{SnO}_2$  layer hinders the transport of liquid Sn and  $\text{O}_2^-$  to the reactive interface. When the LTA-DCFC operates in the  $\text{H}_2$  mode, the  $\text{SnO}_2$  layer can be effectively reduced, considerably enhancing the cell performance. With the cell operating in the CO mode, since the CO diffusion rate in the liquid Sn is much slower than in  $\text{H}_2$ , only part of  $\text{SnO}_2$  was reduced. The OCV was slightly higher than the OCV in battery mode and lower than the OCV in the  $\text{H}_2$  mode, indicating that the cell performance depends on both Sn and CO electrochemical oxidation reactions. When the cell operates in the carbon mode, it is difficult for the carbon to reach the reactive interface between the liquid anode and electrolyte, so the cell performance is mainly governed by the Sn electrochemical oxidation. As it can be seen in Figure 3, after 45 min following carbon addition, the OCV increased from 0.6 to 0.7 V, and after 10 h, it increased to 0.75 V. And the maximum current density improved from 15  $\text{A m}^{-2}$  to 38  $\text{A m}^{-2}$ , indicating that carbon can have small positive impacts on cell performance, reducing part of the  $\text{SnO}_2$  after a longer interval. The results of Khurana et al. [30] were similar. The OCV of 0.841 V for the cell operating in battery mode, close to the theoretical standard potential of 0.85 V at 900 °C, indicates Sn oxidation to  $\text{SnO}_2$ . The increase in the OCV to 1.1 V for the  $\text{H}_2$ -fed cell confirms that  $\text{H}_2$  reduces  $\text{SnO}_2$ . The OCV of the cell following coal injection was 0.885 V, lower than that of the  $\text{H}_2$ -fueled cell, but higher than that of the cell operated in battery mode, attesting that carbon addition led to a partial  $\text{SnO}_2$  reduction.

Summarizing, the expectations of a large-scale development of this type of fuel cell are not high. A challenge is to increase the performance by optimizing the fuel cell structure and operation conditions.

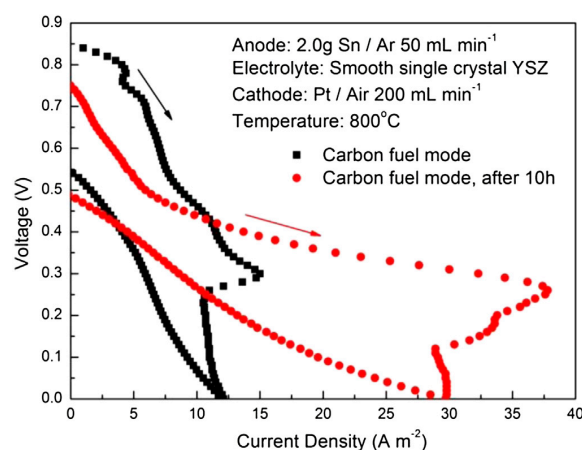


**Figure 3.** Polarization curves for liquid Sn anode in the carbon fuel mode. Reproduced from Ref. [23], copyright 2014, with permission from Elsevier. The arrows indicate the forward scanning curve.

### 2.1.2. Liquid-Tin-Containing-SO-DCFCs

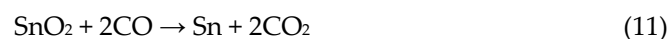
In this case, Sn acts as an “interfacial mediator” to improve the TPB. Some works reported the use of Sn as an “interfacial mediator”, with Ni/YSZ as the anode electrocatalyst and YSZ as the electrolyte [27,32,33]. First, Ju et al. [27] compared the performance of an SO-DCFC operating at 900 °C fueled with pure carbon black and Sn-containing carbon black (Sn:C 1:3 by weight). The maximum power density (MPD) of the Sn/carbon-fed SO-DCFC was more than four times higher than that of carbon-fed SO-DCFC, indicating that the transfer of carbon particles and the kinetics of the electrochemical carbon oxidation are facilitated. Jiang et al. [32] evaluated the effect of the presence of a low Sn amount on SO-DCFC performance. An amount of 15–30 mg of Sn mixed with 300 mg of carbon black was the optimum amount for a suitable interfacial effect. By the addition of 15 mg of Sn, the MPD at 750 and 850 °C was three and two four times higher, respectively, than that obtained with Sn-free carbon black. Conversely, 60 mg of Sn covered the Ni/YSZ surface and pores too thickly, hindering carbon access to the TPB. The OCV of the SO-DCFCs with Sn as the mediator did not follow the theoretical potential of Sn oxidation, but was close to carbon oxidation potential. Xu et al. [33] evaluated the effect of carbon type on the SO-DCFC performance using a high amount of tin (Sn:C 1:0.25 by weight) as a mediator. Graphite (GC), anthracite coal (AnC), lignite (PCF), and activated carbon (AC) were mixed with Sn powder and used as anode fuels. For Sn–GC-, Sn–AnC-, and Sn–PCF-fueled cells, the SnO<sub>2</sub> reduction rate was lower than the electro-oxidation rate of Sn, leading to SnO<sub>2</sub> accumulation on the anode surface. The OCV and MPD at 750–850 °C were similar to those of Sn-only fueled cells, suggesting that the anode performance was mainly governed by Sn electro-oxidation. For Sn–AC-fueled cells, instead, the high-surface-area carbon reduced SnO<sub>2</sub> much faster than the other fuels and no SnO<sub>2</sub> was detected in the anode pores. The power density was considerably higher than that of Sn-only-fueled cells. Two mechanisms were proposed to describe the carbothermal reduction process of SnO<sub>2</sub> formed by reaction (8):



One was the direct reduction of SnO<sub>2</sub> by carbon:



namely, the solid–solid mechanism, and the other was based on two steps: first, the carbon particles are oxidized via the non-electrochemical reverse Boudouard reaction (reaction 5), then SnO<sub>2</sub> is reduced by CO:



namely, the solid–gas mechanism. Based on Levêque and Abanades’s studies [36], Xu et al. [33] inferred that AC reduced SnO<sub>2</sub> through the solid–gas mechanism. Moreover, the OCV of Sn–AC was 1.0–1.03 V, corresponding to the C/CO electro-oxidation potential.

The histogram of OCV and MPD of the SO-DCFC fueled with PCF and AC without and with Sn presence is shown in Figure 4. As can be seen in Figure 4, for PCF, the addition of Sn results in a negative effect on OCV and MPD, while for AC, Sn presence leads to an enhancement of the performance. For PCF, in Sn absence, the cell performance is controlled by carbon oxidation, but in Sn presence, it is controlled by tin oxidation, resulting in a lower OCV; SnO<sub>2</sub> accumulation on the anode surface gives rise to a decrease in SO-DCFC performance. For AC, the cell performance is controlled by carbon oxidation both with and without Sn in the fuel: in this case, no SnO<sub>2</sub> accumulation occurs, and a positive effect of Sn, as an interfacial mediator, takes place on cell performance.



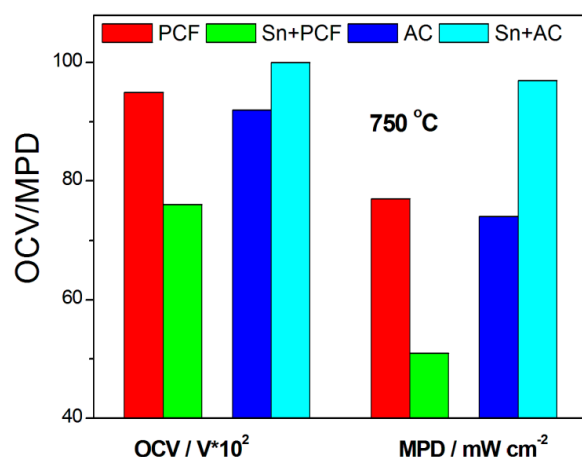
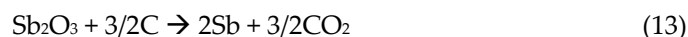


**Figure 4.** The histogram of open-circuit voltage (OCV) and maximum power density (MPD) of the solid oxide–direct carbon fuel cell (SO-DCFC) fueled with lignite (PCF) and activated carbon (AC) without and with Sn presence from data in Ref. [33]. \* is a multiplication sign.

## 2.2. Liquid Antimony Anode–Direct Carbon Fuel Cells (LAA-DCFCs)

Among the metals investigated, antimony is the most promising, as the melting temperatures of both the metal and its oxide are below SO-DCFC operating temperatures, allowing for good contact between the metal and the electrolyte and between the oxide and the carbon fuel. Moreover, the impedance of molten Sb electrodes is very low, less than  $0.1 \Omega \text{ cm}^2$  at  $700^\circ\text{C}$  [26]. Although the Nernst potential for Sb oxidation is lower compared to that for C oxidation,  $0.75 \text{ V}$  vs.  $\sim 1 \text{ V}$  at  $700^\circ\text{C}$ , this difference in oxidation potentials makes the reduction of  $\text{Sb}_2\text{O}_3$  by carbon fuels thermodynamically spontaneous. The anodic reactions are



The liquid  $\text{Sb}_2\text{O}_3$  migrates away from the anode/electrolyte interface, ensuring good contact between molten Sb and electrolyte. As can be seen in Table 1, a stable operation of LAA-DCFCs, fueled with different carbons, is reported, with a power density in the range of  $25\text{--}300 \text{ mW cm}^{-2}$  at a fixed current density or cell potential. An MPD of  $360 \text{ mW cm}^{-2}$  at  $700^\circ\text{C}$  was obtained by a sugar-char-fed LAA-SO-DCFC with a scandia-stabilized zirconia (ScSZ,  $100 \mu\text{m}$ ) electrolyte and a LSF-ScSZ cathode.

Corrosion of the electrolyte by liquid Sb/ $\text{Sb}_2\text{O}_3$  at operating SO-DCFC temperatures is a critical issue. Both of the most used electrolyte materials, that is, stabilized  $\text{ZrO}_2$  and doped  $\text{CeO}_2$ , are prone to corrosion by liquid Sb/ $\text{Sb}_2\text{O}_3$  at temperatures above  $700^\circ\text{C}$ . Jayakumar et al. [13] ascribed the more severe thinning of the ScSZ electrolyte by the liquid metal anode than that of YSZ to the smaller radius of  $\text{Sc}^{3+}$  cations than  $\text{Y}^{3+}$  cations. Zhou et al. [37], instead, reported that the thinning of zirconia-based electrolytes in SOFC with molten Sb anodes is due to chemical reactions between  $\text{Sb}_2\text{O}_3$  and  $\text{ZrO}_2$ , independently of the dopant. Cao et al. [38] investigated liquid Sb anode etching on YSZ and gadolinia-doped ceria (GDC) electrolytes, and observed electrolyte corrosion in both polycrystalline materials. In both cases, Sb migrated along grain boundaries, breaking connections between grains, and damaging the electrolytes. Ma et al. [39,40] observed that YSZ corrosion is different from GDC corrosion. Both liquid Sb and, to a lesser extent,  $\text{Sb}_2\text{O}_3$  penetrate into GDC grain boundaries, resulting in spallation of the grains from the bulk [39]. YSZ corrosion in both liquid Sb and, to a greater extent,  $\text{Sb}_2\text{O}_3$  occurs by Y dissolution, causing a phase transformation in the YSZ surface [40].

The accompanied volume change results in surface cracks along YSZ grain boundaries. The corrosion is enhanced by the presence of a current. Reducing the number of



grain boundaries can be a solution to resist electrolyte corrosion by liquid Sb/Sb<sub>2</sub>O<sub>3</sub>. Cao et al. [41] investigated the corrosion resistance of a ScSZ electrolyte prepared by atmospheric plasma spray (APS) technology. APS technology allows for preparing robust films by melting feed powder in a plasma plume [42]. They tested two LAA-DCFCs with the same electrolyte material but prepared by sintering and APS methods. The etching effect was observed on a sintered electrolyte, but not on a plasma-sprayed electrolyte. As Sb was transported along grain boundaries in a sintered electrolyte, there were ample pathways for Sb migration. Grain boundaries in the plasma-sprayed electrolyte, instead, can hardly be identified. To enhance the corrosion resistance of GDC electrolytes for LAA-DCFCs, different amounts of Fe<sub>2</sub>O<sub>3</sub> were added to GDC, namely GDCF [43]. Fe<sub>2</sub>O<sub>3</sub> addition significantly increased the corrosion resistance of GDC by liquid Sb/Sb<sub>2</sub>O<sub>3</sub>. As can be seen in Figure 5, where the dependence of the depth of the affected layer by liquid Sb at 750 °C for 100 h on Fe<sub>2</sub>O<sub>3</sub> content is reported, the GDCF with 2 mol% Fe<sub>2</sub>O<sub>3</sub> added showed the highest corrosion resistance by liquid Sb: liquid Sb affected a GDC thickness of about 60 µm, which is smaller than 1/8 of that of pure GDC. Moreover, the affected thickness was only about 4 µm for GDC with 2 mol% Fe<sub>2</sub>O<sub>3</sub> in contact with liquid Sb<sub>2</sub>O<sub>3</sub>. Part of the Fe added reacted with GDC, forming Fe<sub>5</sub>Gd<sub>3</sub>O<sub>12</sub>. The GDC with 3 mol% Fe<sub>2</sub>O<sub>3</sub> contained the highest amount of Fe<sub>5</sub>Gd<sub>3</sub>O<sub>12</sub>, favoring the penetration of liquid Sb and explaining its weak corrosion resistance.

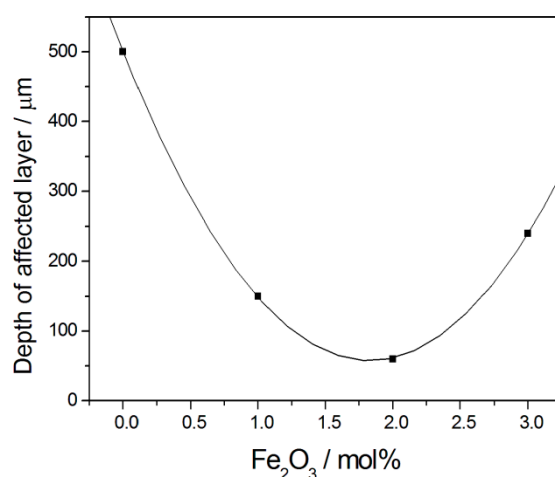


**Figure 5.** Dependence of the depth of affected layer by liquid Sb at 750 °C for 100 h on Fe<sub>2</sub>O<sub>3</sub> content from data in Ref. [43].

As in the case of tin, it should be interesting to carry out tests on liquid-antimony-containing SO-DCFCs, where molten Sb is added to a typical SOFC.

### 3. Hybrid Direct Carbon Fuel Cells (HDCFCs)

#### 3.1. From MH-, MC-, and SO-DCFCs to HDCFCs

The first MH-DCFC dates back to 1896 [44]. Hydroxides have low melting points and high ionic conductivity, allowing the cell to operate at relatively low temperatures and, hereupon, to use less expensive materials [4]. MH-DCFCs, however, received little attention in the last few decades, due to the deterioration of the hydroxide electrolyte during cell operation [45]. Despite a renewal of the research into MH-DCFCs [46–48], the stability of the hydroxide is not satisfactory for practical applications. In 1979, Weaver et al. [49] proposed the use of a fuel cell with a molten carbonate electrolyte for direct carbon conversion, that is, an MC-DCFC. The state-of-the-art MCFC consists of a porous nickel anode; a porous, lithium-doped NiO cathode; and a LiAlO<sub>4</sub> matrix filled with Li/K carbonates as the electrolyte [50]. At the cathode, CO<sub>2</sub> is converted to CO<sub>3</sub><sup>2-</sup> [51]:



Then,  $\text{CO}_3^{2-}$  ions diffuse through the matrix and reach the anode side. At the anode,  $\text{CO}_3^{2-}$  ions reacts with carbon particles, releasing four electrons and  $\text{CO}_2$ :



The net electrochemical reaction is



with four electrons flowing from the anode to the cathode.

Different types of carbons were used as the fuel in MC-DCFCs with appreciable performances [51–55]. However, MC-DCFCs present some problems, such as cell material corrosion by carbonates and a change of chemical composition of solid fuels. Moreover, the molten carbonate can likely change chemically due to its interaction with carbon contaminants, leading to cell failure [56]. Compared with MC-DCFCs and MH-DCFCs, SO-DCFCs have the outstanding advantages of an all-solid-state structure, no electrolyte degradation and leakage, no  $\text{CO}_2$  recirculation from the anode to cathode, and high electrical-conversion efficiency [6]. As previously reported, however, the poor contact between the solid fuel and the solid electrode/electrolyte results in a low cell performance. A way to solve this drawback is to improve the anode structure. It is known that the porosity and microstructure of the anode have an important impact on SOFC performance [57,58].

However, the poor contact problem between the solid fuel and solid anode/electrolyte remains. For these reasons, HDCFCs were proposed. An HDCFC is a combination of an MC-DCFC and an SO-DCFC, and both reactions, that occur at the anode of the MC-DCFC and the SO-DCFC, take place at the anode of the HDCFC [4]. HDCFCs were first proposed by Peelen et al. [59]. This design consists of a solid cathode and solid oxide electrolyte, and a molten alkali carbonate–solid carbon slurry in the anode chamber [60]. The schematic configuration of an HDCFC is shown in Figure 6. The following reactions take place in the anode chamber [61]: (i) electrochemical oxidation of carbon by  $\text{O}^{2-}$  ions, according to reactions 2 and 3; (ii) electrochemical oxidation of carbon by  $\text{CO}_3^{2-}$  ions, according to reaction 15, 17, and 18:

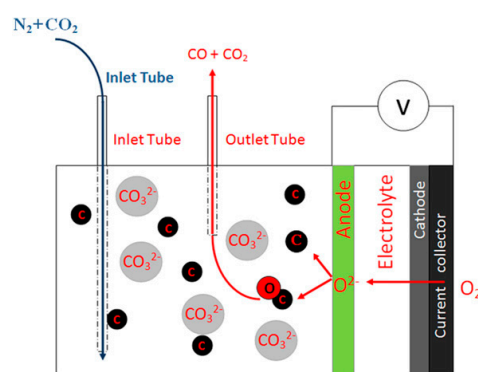
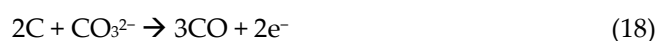
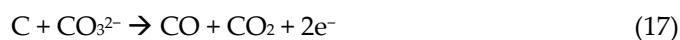


**Figure 6.** Schematic configuration of Hybrid Direct Carbon Fuel Cell. Reproduced from Ref. [60], copyright 2012, with permission from Elsevier.



(iii) electrochemical oxidation of CO, according to reactions 4 and 19:



(iv) the non-electrochemical reverse Boudouard reaction.

Moreover, the non-electrochemical carbonate decomposition can also occur as [62,63]



Due to the additional carbon oxidation by carbonate, the OCV is expected to increase to 1.22 V at 700 °C [64]. Jiang and Irvine [65] observed that the OCV not only depends on thermal history, but also on carbonate amount in the carbon/carbonate slurry. Heat treatment was effective for high carbonate contents. After high-temperature treatment with 50 mol% carbonate, the OCV increased with decreasing temperature and reached 1.57 V at 550 °C. With a lower carbonate content (20 mol%), instead, the OCV decreased with decreasing temperature. The high OCV was also ascribed to the Li<sub>2</sub>O presence, formed by Li<sub>2</sub>CO<sub>3</sub> decomposition at high temperatures [66]. Li<sub>2</sub>O can trap the formed CO<sub>2</sub>, decreasing its activity and improving the OCV.

As for conventional DCFCs [67], HDCFCs can be categorized on the basis of the material and design of anode, that is, a molten carbonate/fuel mixture, a solid catalyst anode, and a molten metal anode.

### 3.2. HDCFCs with a Liquid Carbonate/Carbon Anode

First, at SRI, a new type of DCFC was proposed [68], which is basically a tubular SOFC, without the traditional SOFC solid anode catalyst. This type of fuel cell is formed by a liquid anode, comprising a molten Li/Na/K carbonate mixture and the fuel (coal powder, ca., 40 vol%), an YSZ electrolyte, and a lanthanum strontium manganite (LSM) cathode catalyst. The immersion of coal powder in molten carbonates solves the drawback of the poor contact between the solid fuel and the electrolyte [69]. This HDCFC delivered an MPD above 100 mW cm<sup>-2</sup> at 950 °C. Then, the performance of the SRI tubular HDCFC was evaluated by EPRI using two types of fuel, that is, coal and carbonized biomass. For both fuels, a power density of 90–100 mW cm<sup>-2</sup> was attained at 790 °C. Prolonged exposure of the fuel cell at 600–700 °C to the molten salt/fuel slurry did not reveal appreciable degradation of the electrolyte. After these preliminary works, some papers were addressed to an HDCFC with a liquid carbonate/carbon anode [70–73]. In all these works, a planar HDCFC with a composite electrolyte was formed by samarium-doped ceria (SDC) and eutectic Li/Na carbonates, and a LiNiO<sub>2</sub>/electrolyte (70/30 wt%) composite cathode was tested. The carbon/carbonate weight ratio was 1:9. Jia et al. [70] put a mixture of activated carbon and molten carbonates in the anode cavity. With a CO<sub>2</sub>/O<sub>2</sub> ratio of the cathode gas of 2:1, an MPD of 100 mW cm<sup>-2</sup> was obtained. Elleuch et al., using anodes formed by a mixture of graphite powder [71], almond shell biochar [72], or olive wood charcoal [73] and molten carbonates, attained MPD values of 58 mW cm<sup>-2</sup> at 700 °C, 127 mW cm<sup>-2</sup> at 750 °C, and 105 mW cm<sup>-2</sup> at 700 °C, respectively.

### 3.3. HDCFCs with a Solid Catalyst Anode

As previously reported, molten carbonates bring the oxygen ions to the coal particles to complete the cell reactions. The reaction rate, however, is low, so the presence of a catalyst can be helpful to improve it. The anode catalyst provides suitable sites for carbon electro-oxidation, and delivers the produced electrons to the current collectors [74]. To evaluate the effect of the presence of a solid anode, Cantero-Tubilla et al. [75] compared the performance of two identical HDCFCs, fueled with the same carbon/carbonate mixture, one with a GDC anode catalyst and the other without an anode catalyst. In the absence of a catalyst, the MPD was 7 mW cm<sup>-2</sup>, regardless of the operating temperature. In the presence of a dense GDC catalyst, the MPD at 800 °C increased more than 500%. Conversely, Xu et al. [76] reported that the performance of an HDCFC without an anode catalyst was better than with a Ni/SDC anode catalyst. This comparison, however, is not appropriate. Indeed, the HDCFC with a NiO/SDC catalyst and Ag paste as the current collector cannot be compared to the HDCFC without an anode catalyst, but with Cu foil

immersed in the carbon/carbonate mixture as the current collector: indeed, the Cu foil also acts as an anode catalyst, with Cu as an active catalyst for the carbon/carbonate fuel [77]

As for the SOFCs, from a geometrical point of view, HDCFCs can be mainly classified into a planar cross-flow and tubular counter-flow type [78,79]. There are various structural configurations of SOFCs, including anode-, cathode-, and electrolyte-supported SOFCs [80]. Generally, HDCFCs were fabricated in anode- or electrolyte-supported configurations [81]. Jiang et al. [65] compared the performance of electrolyte- and anode-supported HDCFCs. The MPD increased from 70 to 390 mW cm<sup>-2</sup> at 750 °C under N<sub>2</sub>, changing the cell configuration from a 1 mm-thick YSZ electrolyte-supported structure to an anode-supported structure with a 5 µm-thick YSZ electrolyte, due to the lower ohmic resistance of the electrolyte. Gil et al. [81] compared the performance of a cathode-supported HDCFC—which has the advantage of the use of a thin anode layer to promote the full contact between the fuel and the anode, together with the use of a thin electrolyte, maintaining a low ohmic resistance—to that of a conventional anode-supported HDCFC. The performance of the cathode-supported HDCFC was 1.7 times higher than that of the anode-supported cell. Notwithstanding the advantages of the cathode-supported configuration, the manufacturing of this type of cell remains extremely challenging.

Literature data on solid-catalyst-based HDCFCs are reported in Table 2 [60–62,64,65,74–77,81–107]. The histograms in Figure 7 show the number of papers for the various types of anode and cathode catalysts, and of the electrolyte used in HDCFCs.

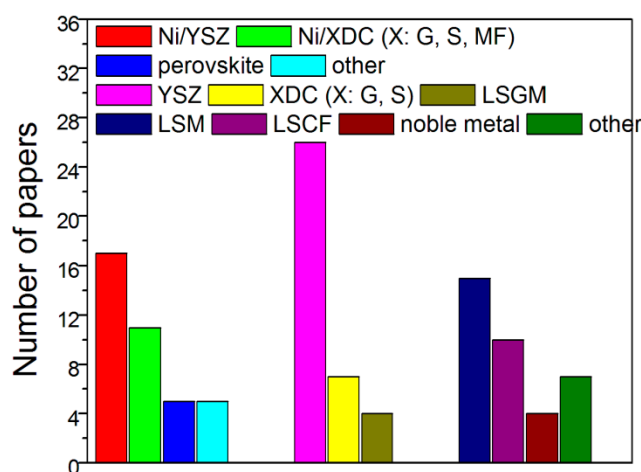


**Figure 7.** Histograms of the number of papers for the various types of anode and cathode catalysts, and of the electrolyte used in hybrid direct carbon fuel cells from data in references reported in Table 2 in the year range of 2006–2023.

**Table 2.** Some literature data of solid-catalyst-anode-based HDCFCs, including intrinsic parameters (catalysts and electrolyte), operational parameters (type of fuel, carbon/carbonate composition, and temperature), and MPD values. The results are sorted by increasing year. \* The values of power were not normalized by surface area, because the type of flux of carbonate and carbon in tubular geometry is dynamic rather than static.

Fuel//Carbonate Ratio	Anode//Electrolyte//Cathode	T °C	MPD mW cm <sup>-2</sup>	Refs
S carbon black//Li/K 62/38% 8:1 molar	Ni mesh//YSZ//Pt	700	10 mW (not normalized) *	[82]
S carbon black//Li/K 62/38% 1:1 molar, 1.9 g	NiO/YSZ//YSZ//LSM/YSZ	700	0.5 (no carbonate)	[62]
XC carbon black//Li/K 62/38% 1:1 molar ratio, 1.9 g		900	3.6	
		700	15.5 (no carbonate)	
		900	13	
			6.4	
			12.6	
Ni-carbon black//Li/K 62/38% 1:1 molar	NiO/YSZ//YSZ//LSM/YSZ	550	0.16 (Ni 0 wt%)	[64]
		700	1.18 (Ni 50 wt%)	
			2.2 (Ni 0 wt%)	
			5.8 (Ni 50 wt%)	
XC carbon black//Li/K 62/38% 4:1 molar	NiO/YSZ//YSZ//LSM/YSZ	700	20	[65]
		800	50	
Pirolized MDF//Li/K 62/38% 4:1 weight	NiO/YSZ//YSZ//LSM/YSZ NiO/YSZ//YSZ//LSCF/GDC	750	70 (electrolyte-supported) 390 (anode-supported, N <sub>2</sub> ) 500 (CO <sub>2</sub> purge gas) 878 (flowing air cathode)	[83]
Pirolized MDF//Li/K 62/38% 4:1 molar	NiO/GDC//GDC//LSM/GDC	700	40 mW (not normalized) *	[60]
		750	90 mW (not normalized) *	
carbon black//Li/K 62/38% 4:1 weight	-//YSZ//LSCF/GDC denseGDC//YSZ//LSCF/GDC dense/porousGDC//YSZ//LSCF/GDC	775	7 42 70	[75]
graphite (<20 µm)//Li/K 62/38% 1:1 molar	NiO/SDC//SDC//Ba <sub>0.5</sub> Sr <sub>0.5</sub> Co <sub>0.8</sub> Fe <sub>0.2</sub> O <sub>3-δ</sub> (BSCF) PorousSDC//SDC//BSCF NiO/SDC//SDC//BSCF -//SDC//BSCF		37	[76]
activated carbon (125–250 µm, AC250)//Li/K 62/38%. 1:1 molar		650	41	
			89	
			113	
		650	40	
		700	63	
German creek (200 µm) (GK200)		750	85	
Graphite carbon (20 µm) (GC20)		650	42	
Activated carbon (70 µm) (AC70)		700	75	
Activated carbon (250 µm)	NiO/SDC//SDC//BSCF	750	113	[84]
Activated carbon (500 µm)		650	60	
For all carbons C//Li/K 62/38%		700	100	
1:1 molar		750	132	
		750	158	
		750	126	
Activated Carbon (XC-72R)//Li/K 62/38%. 1:1 weight	NiO/YSZ//YSZ//LSCF	700	37 (after 17 h at 0.7 V)	[85]
Pirolized MDF//Li/K 62/38%		800	53 (after 17 h at 0.7 V)	
//Ni(NO <sub>3</sub> ) <sub>2</sub> , 4:1:1		800	92 (after load at 0.8 V, no gas flow)	
Almond shell biochar/Li/Na 66/33%. 1:9 weight	NiO/SDC//SDC//Li/Na 66/33%(70:30wt%)/Li <sub>x</sub> Ni <sub>1-x</sub> O	600	20	[74]
		650	64	
		700	148	
Anthracite coal	Cu/CeO <sub>2</sub> //YSZ//Ag	750,800	1.2 (all MPD under 3.7 CO <sub>2</sub> flow)	[77]
Bituminous coal		750	2.7	
		800	4.8	
Demineralized bituminous coal		750	3.3	
Pine Charcoal		800	5.3	
For all carbons C//Li/K 62/38%		750	7	
4:1 weight		800	12	
Carbon black//Li/K 62/38%/-	NiO/YSZ//YSZ//LSM/YSZ		22	[86]
Carbon black//Li/K 62/38%//Ag <sub>2</sub> O 4:1:1 weight		800	58	

Graphite				
Anthracite coal milled			67 (all PD at 0.5 V)	
Anthracite coal milled demineral			97	
Bituminous coal milled			103	
Bituminous coal milled deminer	NiO/13YSZ//YSZ//LSM/YSZ	700	115	[87]
Pine Charcoal			165	
Activated Carbon (XC-72R)			96	
For all carbons C//Li/K 62/38%			145	
4:1 weight				
		750	127	
	NiO/YSZ//YSZ//LSM/YSZ	850	265	
Carbon Super P//Li/K 62/38%	PorousNiO <sup>a</sup> /YSZ//YSZ//LSM/YSZ	750	105	
1:1.5 weight	PorousNiO <sup>b</sup> /YSZ//YSZ//LSM/YSZ	850	359	[88]
	SA PorousNiO <sup>a</sup> > SA PorousNiO <sup>b</sup>	750	80	
		850	287	
		600	32	
Corn cob biochar/Li/Na 66/33%. 1:9 weight	NiO/SDC//SDC/Li/NaCO <sub>3</sub> (70:30wt%)/Li <sub>x</sub> Ni <sub>1-x</sub>	650	68	
	O	700	113	[89]
		750	185	
Anthracite coal				
Carbonized anthracite coal			45	
Bituminous coal	NiO/YSZ//YSZ//LSM/YSZ	750	45	
Carbonized bituminous coal			68	[90]
For all carbons C//Li/K 62/38%			40	
4:1 weight				
Carbon black				
Bituminous coal			118	
Torrefied switchgrass			94	
Pyrolyzed switchgrass (charcoal)	dense/porousGDC//YSZ//LSCF/GDC	800	121	
Torrefied hardwood			102	[91]
Torrefied corn stover			118	
For all carbons C//Li/K 62/38%			110	
16:1 volume				
Magazine paper carbon			172	
Newspaper carbon			136	
Activated charcoal	NiO/SDC//SDC//LSCF	650	93	[92]
C//Li/K/Na 32/35/33%				
1:1 weight				But lower durability than AC
Anthracite coal I (low volatile)				
Anthracite coal II (low volatile)			60	
Bituminous coal I (low ash)	NiO/YSZ//YSZ//LSM/YSZ	750	58	
Bituminous coal II (low ash)			62	[93]
For all carbons C//Li/K 62/38%			72	
4:1 weight				
Pyrolyzed organic xerogel				
Bituminous coal II	(La, Sr)(Cr, Mn)O <sub>3</sub>		45	
Pyrolyzed organic xerogel	(LSCM)-GDC//YSZ//LSM/YSZ/LSM	750	60	[94]
For all carbons C//Li/K 62/38%	NiO/YSZ//YSZ//LSM/YSZ/LSM		23	
4:1 weight				
		700	5 (no carbonate)	
			10.7	
		750	9.2 (no carbonate)	
			18.2	
		800	13.2 (no carbonate)	
Lignite	Co/CeO <sub>2</sub> //YSZ//Ag		22.8	
Lignite 800			7.1 (no carbonate)	[95]
		700	12.7	
		750	12.2 (no carbonate)	
			20.9	
			15.3 (no carbonate)	
		800	25.5	
Activated carbon	NiO/YSZ//YSZ//LSCF/GDC	700	79 (N <sub>2</sub> purge gas)	[96]
Carbon black		800	535	

Graphite For all carbons C//Li/K 62/38% 4:1 molar			700	155 (CO <sub>2</sub> purge gas)	
			800	489	
			700	21 (N <sub>2</sub> purge gas)	
			800	224	
			700	38 (CO <sub>2</sub> purge gas)	
			800	380	
			700	28 (N <sub>2</sub> purge gas)	
			800	154	
Activated carbon//Li/K 62/38% 4:1 weight	SFXM//LSGM//LSFC SFXM (Sr <sub>2</sub> Fe <sub>1.4</sub> X <sub>0.1</sub> Mo <sub>0.5</sub> O <sub>6-δ</sub> , X = Bi, Al, Mg)		700	141 (SFBM anode)	[97]
			750	287	
			800	399	
			800	293 (SFAM anode)	
			800	181 (SFMM anode)	
Graphite//Li/K 62/38% 4:1 weight	3D NiO/GDC//GDC-Li/Na <sub>2</sub> CO <sub>3</sub> // Sm <sub>0.5</sub> Sr <sub>0.5</sub> CoO <sub>3</sub> (SSC)		500	143	[98]
			550	196	
			600	325	
Carbon black//Li/K 62/38% 4:1 weight	NiO/YSZ//YSZ//LSM/YSZ		755	44 (anode-supported)	[81]
				75 (cathode-supported)	
Activated carbon//Li/K 62/38% 4:1 weight	Ni(50%)-Ce <sub>0.6</sub> Mn <sub>0.3</sub> Fe <sub>0.1</sub> O <sub>2</sub> (Ni-CMF)cermet/SDC//LSGM//LSCF CMF//LSGM//LSCF		700	227	[99]
			750	478	
			800	581	
			800	172	
Activated carbon//Li/K 62/38% 4:1 weight	Ni-CMFnanofibers//LSGM//LSCF	800		230 (0% Ni)	[100]
				320 (22% Ni)	
				530 (30% Ni)	
				370 (30% Ni)	
				200 (58% Ni)	
Pyrolyzed sawdust//Li/K 62/38% Various C/carbonate ratios	Ni/YSZ//YSZ//GDC/LSCF/GDC	750		550(40% carbon) (CO <sub>2</sub> )	[101]
				731 (50% carbon)	
				750 (60% carbon)	
				600 (80% carbon)	
				306 (40% carbon) (N <sub>2</sub> )	
				388 (50% carbon)	
				384 (60% carbon)	
Bituminous coal//Li/K 62/38%//Co/CeO <sub>2</sub> C/carbonate/Co x:y:z weight	Co/CeO <sub>2</sub> //YSZ//Ag	700 800		344 (80% carbon)	[102]
				6.0 (4:0:0)	
				7.2 (4:0:1)	
				7.7 (4:2:0)	
				10.9 (4:2:1)	
				15.5 (4:0:0)	
				17.7 (4:0:1)	
				20.2 (4:2:0)	
Graphite carbon Carbon black Pyrolyzed biomass (charcoal) For all carbons C//Li/K 62/38% 4:1 weight	NiO/YSZ//YSZ//LSM/YSZ	750		24.7 (4:2:1)	[103]
				49	
				25	
				52	
Bituminous coal Charcoal (by pyrolysis BiC) Modified charcoal (acid-treated) For all carbons C//Li/K 62/38% 4:1 weight	NiO/YSZ//YSZ//SDC/ SrSc <sub>0.175</sub> Nb <sub>0.025</sub> Co <sub>0.8</sub> O <sub>3-δ</sub> (SSNC) Ag/NiO/YSZ//YSZ//SDC/SSNC	750		282	[104]
				297	
				366	
				403	
Activated carbon//Li/K 62/38% 4:1 weight	(PrBa) <sub>0.95</sub> Fe <sub>1.8-2x</sub> Cu <sub>x</sub> Nb <sub>0.2</sub> O <sub>5+δ</sub> (PBFCN)//YSZ//LSM/YSZ	800		210 (x = 0.1)	[105]
				275 (x = 0.2)	
				325 (x = 0.3)	
				431 (x = 0.4)	
Activated carbon//Li/K 62/38% 4:1 weight	PorousPBFCN//YSZ//LSM/YSZ	800		765 (x = 0.4)	[106]
Anthracite 250 mesh/ Li/K 62/38% 7:3 weight	metal foam/NiO/SDC //YSZ//SDC SSNC	750		306 (no metal foam)	[61]
				349 (30 PPI Ni foam)	



			389 (90 PPI Ni foam)	
			378 (CuNi foam)	
Activated carbon//Li/K 62/38% 4:1 weight	Sr <sub>2</sub> Fe <sub>1.5</sub> Mo <sub>0.5</sub> O <sub>6-δ</sub> (SFM) //LSGM//LSCF Sr <sub>2</sub> Fe <sub>1.3</sub> Cu <sub>0.2</sub> Mo <sub>0.5</sub> O <sub>6-δ</sub> (SFCM) //LSGM//LSCF	650	51	[107]
		700	92	
		750	143	
		800	286	
		650	100	
		700	156	
		750	315	
		800	489	
Activated carbon//Li/K 62/38% 7:3 weight	Pd/GDC-Ni-Cu/GDC //YSZ-GDC//LSCF/GDC	750	556	[108]

### 3.3.1. HDCFC Anode

As can be seen in Figure 7, Ni-YSZ cermet was the most used anode catalyst in HDCFCs; this catalyst, however, is subjected to various drawbacks, such as sintering, poor redox stability, and low tolerance to coke deposition. Another problem regarding Ni-YSZ is the poor stability of YSZ in molten carbonate [82]. This leads to the degradation of both YSZ mechanical properties and conductivity at temperature < 700 °C. One answer to this problem is to switch to an alternative carbonate mixture: it was found that YSZ is stable in Na/K carbonate eutectic [82], but the HDCFC performance was lower than with Li/K carbonate eutectic [75]. Another way to solve this drawback is to use doped ceria as an alternative to YSZ. The GDC structure seems to be stable in molten Li/K carbonates over 168 h at 500 °C [109]. Xu et al. [110] compared the stability of YSZ and SDC in molten carbonates. They found that SDC was more corrosion-resistant in the molten carbonate eutectics than YSZ. On these bases, GDC, SDC, and also Ce<sub>0.6</sub>Mn<sub>0.3</sub>Fe<sub>0.1</sub>O<sub>2</sub> (CMF) were investigated as Ni supports in HDCFCs [60,61,74,76,84,92,98–100]. A disadvantage of doped ceria, however, is that at high temperature and low oxygen partial pressure, its behavior changes from total ionic conductivity to partial electronic conductivity.

Due to the limited contact between solid carbon fuels and the anode during HDCFC operation, notwithstanding the presence of carbonate, the commonly used Ni anode framework may not be suitable for carbon fuels with a particle size much larger than the anode pore size [111]. Thus, a more efficient anode structure should be designed to improve the reactivity of carbon and the electrochemical performance. Lee et al. [88] modified the anode microstructure (pore volume and surface area). The MPD increased with increasing surface area but was not correlated with the pore volume. In this case, the carbon particle size was always larger than the pore size, so they cannot penetrate into the pores. This behavior, however, is not general, as the performance depends on the ratio of carbon size to anode pore size: Wu et al. [98] tested a 3D NiO-GDC anode in an HDCFC. The 3D anode framework significantly extended the active zone for the electrochemical carbon oxidation. The graphite-fueled HDCFC with this anode achieved an MPD of 325 mW cm<sup>-2</sup> at 600 °C.

A problem regarding the use of Ni-based anode catalysts in HDCFCs is related to the dissolution of Ni and NiO into molten carbonates [50,112]. In addition, as in SO-DCFCs, Ni is poisoned by sulfur present in raw coal fuels [113,114], leading to a significant reduction in cell performance. Due to their excellent sulfur poisoning tolerance, perovskite oxides have attracted considerable attention. Double perovskites showed high catalytic activity when used as anode catalysts in SOFC fueled with hydrogen and low-molecular-weight hydrocarbons [115], so they were tested in HDCFCs [94,97,105–107]. Yue et al. [94] investigated a (La, Sr)(Cr, Mn)O<sub>3</sub> (LSCM) perovskite-GDC composite material as an alternative anode in HDCFCs and investigated its chemical stability in a carbon/molten carbonate mixture at 700–800 °C. The HDCFC with the GDC-LSCM anode showed a significantly higher performance than that with the Ni-YSZ anode, as a result of the high conductivity and high electro-catalytic properties of LSCM-GDC, as well as a high impurity tolerance. LSCM is not stable in a reducing environment, but the impreg-

nation with GDC fine particles protects it from Li attack, enhancing LSCM anode stability.

### 3.3.2. HDCFC Electrolyte

To effectively operate in SOFCs, the electrolyte has to possess high ionic conductivity and electronic insulation [116]. The electrolyte has to have good chemical compatibility with anode and cathode catalysts, and the thermal expansion coefficient (TEC) of the electrolyte has to be in close proximity to that of the electrode catalysts, to avoid cell cracking [84]. As can be seen in Table 2 and Figure 7, YSZ is largely the most used electrolyte, overall due to its good compatibility with Ni cermets, commonly used as the anode catalyst in HDCFCs. Ceria-based electrolytes were also used in HDCFCs at temperatures  $\leq 650$  °C, where the electronic conductivity is acceptable for fuel cell application [116]. Lanthanum strontium gallium magnesium oxide ( $\text{La}_{0.8}\text{Sr}_{0.2}\text{Ga}_{0.8}\text{Mg}_{0.2}\text{O}_{3-\delta}$ , LSGM) perovskite showed a high ionic conductivity, five times higher than that of YSZ, negligible electronic conductivity, and high chemical stability over a wide range of oxygen partial pressures, so it fulfills the requirements for its use as an SOFC electrolyte [117]. A drawback is its reactivity with nickel. Indeed, it was found that the interfacial reaction between Ni-SDC and LSGM can give rise either to the formation of high-resistivity compounds, such as  $\text{LaSrGa}_3\text{O}_7$ ,  $\text{LaSrGaO}_4$  and  $\text{LaNiO}_3$  [118], or the formation of fine MgO particles near the Ni-SDC/LSGM interface [119], leading to an increase in the ohmic resistance. Thus, the use of LSGM in HDCFCs with Ni-based anodes was limited. However, Liu et al. [99,100] used LSGM as the electrolyte with a Ni-cermet anode catalyst in HDCFCs, either inserting an SDC interlayer between the anode and the electrolyte, which prevented a chemical reaction between Ni and LSGM [99], or using a Ni-infiltrated catalyst into the CMF nanofiber anode [100]. On the other hand, LSGM, being chemically compatible and having a compatible TEC with perovskites oxides [120–122], was used in HDCFCs with a doped SFM perovskite as the anode catalyst [106,107].

A drawback peculiar to HDCFCs is the stability of solid electrolytes in contact with corrosive molten carbonates. Jiang et al. [83] reported a significant YSZ intergrain erosion under oxidizing conditions. Conversely, under reducing conditions, a good stability of YSZ was observed. Xu et al. [110] carried out high-temperature corrosion tests of YSZ and SDC in molten Li/K carbonate eutectic in air at 700 °C for 10 days of testing. The results confirmed YSZ and SDC corrosion, but YSZ was less corrosion-resistant than SDC.

### 3.3.3. HDCFC Cathode

As can be seen in Table 2 and Figure 7,  $\text{La}_{1-x}\text{Sr}_x\text{MnO}_3$  (LSM) perovskites are the most used cathode materials in HDCFCs. The oxygen ion conductivity of LSM materials, however, is low, limiting the use of LSM cathodes at operating temperatures  $\leq 800$  °C [123,124]. Due to its high oxygen ion conductivity,  $\text{La}_{0.6}\text{Sr}_{0.4}\text{Fe}_{0.8}\text{Co}_{0.2}\text{O}_3$  (LSFC) is a promising candidate for SOFCs working at temperatures  $\leq 800$  °C [123,124]. For this reason, LSFC was widely used as the cathode catalyst in HDCFCs. However, LSFC perovskites are generally incompatible with YSZ electrolytes, as LSFC reacts with YSZ to form an  $\text{SrZrO}_3$  insulating phase at 800 °C [123,124]. Thus, a GDC diffusion barrier layer is commonly used to avoid the reaction between LSFC and YSZ [123,124]. On the other hand, LSFC is compatible with LSGM, and in HDCFCs, when LSGM was used as the electrolyte, LSFC was always used as the cathode catalyst. Precious metals (Pt and, in particular, Ag),  $\text{Li}_x\text{Ni}_{1-x}\text{O}$ , and other perovskite oxides, such as  $\text{SrSc}_{0.175}\text{Nb}_{0.025}\text{Co}_{0.8}\text{O}_{3-\delta}$  (SSNC) and  $\text{Ba}_{0.5}\text{Sr}_{0.5}\text{Co}_{0.8}\text{Fe}_{0.2}\text{O}_{3-\delta}$  (BSCF), were also used as cathode catalysts in HDCFCs.

### 3.3.4. Effect of Carbonate Presence (HDCFC vs. SO-DCFC) and Carbon/Carbonate Ratio

To evaluate the effect of carbonate presence, the performance of HDCFCs and SO-DCFCs with the same intrinsic and operational parameters was compared in different works [62,75,77,88,95,99]. In almost all the cases, the performance of the cell with car-

bonate was higher than without, due to the extension of the reaction zone. The dependence of the ratio of the MPD of HDCFC to MPD of SO-DCFC ( $\text{MPD}_{\text{HDCFC}}/\text{MPD}_{\text{SO-DCFC}}$ ) on the operating temperature from data in refs. 62,77,88,95, and 99 is shown in Figure 8a.

The  $\text{MPD}_{\text{HDCFC}}/\text{MPD}_{\text{SO-DCFC}}$  ratio decreases with increasing operating temperature. In addition to temperature, the  $\text{MPD}_{\text{HDCFC}}/\text{MPD}_{\text{SO-DCFC}}$  ratio also depends on the type of carbon. The dependence of the  $\text{MPD}_{\text{HDCFC}}/\text{MPD}_{\text{SO-DCFC}}$  ratio on temperature for raw and heat-treated lignite is shown in Figure 8b. After heat treatment, the carbon content in lignite increased, whereas the volatile matter, such as moisture, sulfur, and oxygen contents, decreased. As a consequence, an improvement in the performance of both SO-DCFC and HDCFC fueled with heat-treated lignite than the cells fueled with raw lignite was observed. In the 700–800 °C temperature range, the  $\text{MPD}_{\text{HDCFC}}/\text{MPD}_{\text{SO-DCFC}}$  ratio linearly decreased with increasing temperature for both raw- and heat-treated lignite-fed cells. The dependence of the  $\text{MPD}_{\text{HDCFC}}/\text{MPD}_{\text{SO-DCFC}}$  ratio on temperature for the cell fed with raw lignite ( $d(\text{MPD}_{\text{HDCFC}}/\text{MPD}_{\text{SO-DCFC}})/dT = -0.0041 \text{ mW cm}^{-2} \text{ }^{\circ}\text{C}^{-1}$ ), however, was considerably higher than that of the cell fueled with heat-treated lignite ( $-0.0012 \text{ mW cm}^{-2} \text{ }^{\circ}\text{C}^{-1}$ ). Obviously, at a fixed temperature, the values of the  $\text{MPD}_{\text{HDCFC}}/\text{MPD}_{\text{SO-DCFC}}$  ratio depends on the type of carbon. In the 700–800 °C temperature range, the  $\text{MPD}_{\text{HDCFC}}/\text{MPD}_{\text{SO-DCFC}}$  ratio for the cell fueled with raw lignite was always higher than that of the cell fueled with heat-treated lignite. Kaklidis et al. [77] compared the performance of SO-DCFC and HDCFC fueled with various carbons at 800 °C. For both SO-DCFC and HDCFC, the order, in terms of MPD, was pine charcoal (PCC) > demineralized bituminous coal (DBiC) > bituminous coal (BiC) > anthracite coal (AnC). When employing AnC and BiC as fuels in HDCFCs, the power output was almost doubled compared to SO-DCFCs. In the case of the PCC sample, instead, the MPD only slightly increased from 12 to 12.6  $\text{mW cm}^{-2}$ . This result and that for raw and heat-treated lignite seem to indicate that the positive effect of carbonate presence is more pronounced when a less performing fuel is employed. Moreover, the value of the  $\text{MPD}_{\text{HDCFC}}/\text{MPD}_{\text{SO-DCFC}}$  ratio at a fixed temperature depends on carbon/carbonate ratio. As can be seen in Table 2, the most used carbon/carbonate weight ratio in HDCFCs was 4:1 (20 wt% carbonate), independently of the carbon characteristics. The optimum carbon/carbonate ratio used in an HDCFC was evaluated in some works [75,101,125]. Cantero-Tubilla et al. [75] evaluated the effect of carbonate content in the carbon/carbonate mixture (0,2.5,6,9.5,13, and 22 vol % carbonates, corresponding to 0,10,20,30,40, and 60 wt%) on HDCFC performance at 800 °C, using Li/K carbonate eutectic and carbon black as the fuel. A maximum value of the  $\text{MPD}_{\text{HDCFC}}/\text{MPD}_{\text{SO-DCFC}}$  ratio was attained at a carbonate content of 20 wt%, as shown in Figure 8c. The main role of the molten carbonate solution is to uniformly wet the carbon fuel and electrolyte, providing a medium for carbon transport and electrochemical reaction. Depending on the concentration of carbonate, the HDCFC will most likely go from a liquid/solid and/or liquid/gas phase reaction mechanism to a solid/solid and/or solid/gas phase mechanism at the anode. This change in reaction mechanism depends on the distribution of the carbonates in the anodic mixture, since carbonate percolation controls the probability of forming a liquid solution within the anode. From the theoretical calculation based on the model of Malliaris and Turner [126], the minimum percolation threshold was 8.7 vol% carbonate. Thus, the highest kinetics of the electrochemical reaction for the range of compositions investigated by Cantero-Tubilla et al. [75] has to be between 6 and 9.5 vol% carbonate. For this reason, for carbonate loadings <6 vol%, a remarkable drop in MPD was observed. The decrease in the performance above 6 vol% carbonate was ascribed to the increase in the charge-transfer resistance. Li et al. [101], using Li/K carbonate eutectic and pyrolyzed sawdust as the fuel, obtained the best performance for a carbonate content of 40–50 wt%. The different optimal carbonate content essentially depends on the porosity and particle size of the carbon fuel: the higher the carbon surface area, the higher the amount of carbonate needed to wet the carbon surface. Finally, Jiang et al. [125] tested various amounts (10,25 and 40 wt%) of ternary Li/K/Na carbonate in

HDCFCs in terms of cell resistance, cell performance, and durability. The best performance was obtained for the HDCFC operating at 700 °C with 40 wt% carbonate.

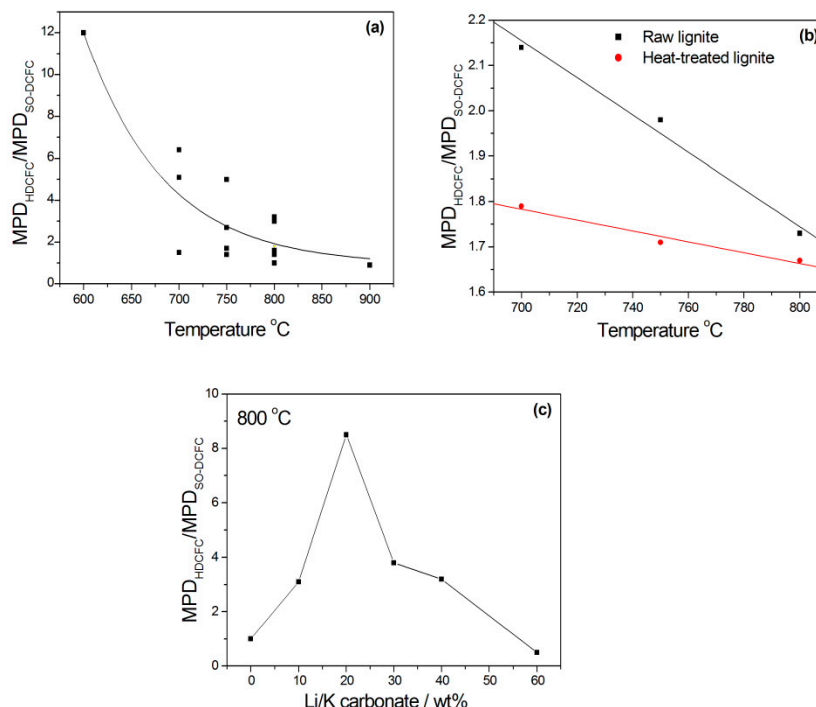


**Figure 8.** (a) Dependence of the ratio of maximum power density (MPD) of hybrid direct carbon fuel cell (HDCFC) to MPD of solid oxide–direct carbon fuel cell (SO-DCFC) ( $MPD_{HDCFC}/MPD_{SO-DCFC}$ ) on operating temperature from data in Refs. [62,77,88,95,99]; (b) dependence of the  $MPD_{HDCFC}/MPD_{SO-DCFC}$  ratio on temperature for raw and heat-treated lignite from data in Ref. [95]; (c) dependence of the  $MPD_{HDCFC}/MPD_{SO-DCFC}$  ratio on carbonate content in the fuel from data in Ref. [75].

### 3.3.5. Effect of the Type of Carbon

Different carbon materials have been used as the fuel in MC-DCFCs [49,52,54,127–131] and SO-DCFCs [132–137]. Generally, a high surface area and a small particle size of carbon fuel can improve its electrochemical reactivity by increasing the interaction between the carbon particles and the anode catalyst. Conversely, a high graphitic degree of carbon fuel can lead to a lower electrochemical reactivity due to the less reactive sites on the carbon surface. Moreover, the electrochemical reactivity of carbon fuels increases with increasing concentration of oxygen-containing functional groups on their surface.

As previously reported, in some works comparing HDCFCs and SO-DCFCs, the order of reactivity of different carbons was the same [77,102]. The increase in the power density was correlated with the increase in porosity and structure disorder. Conversely, high ash and sulfur contents hindered the electrochemical performance. The performance of various types of carbons as fuels in HDCFCs was compared in many works [76,84,87,90,92–94,96,104]. Generally, among various carbons, the HDCFC fueled with AC showed the highest MPD. The higher performance of AC was ascribed to its disordered structure and higher surface area, promoting CO formation via the reverse Boudouard reaction. Moreover, the mesoporous and macroporous structure of AC enhances the transport of carbonates through the carbon skeleton and leads to more active reaction sites. To investigate the effect of the size of carbon on the electrochemical performance, three activated carbons with different sizes (AC (70  $\mu\text{m}$ ), AC (250  $\mu\text{m}$ ), and AC (500  $\mu\text{m}$ )) were used as the fuel in an HDCFC [84]. Independently of carbon size, the HDCFC operating at 750 °C showed a similar OCV. The HDCFC with the middle-size AC as the fuel

delivered the highest power density. As shown in Figure 9, the dependence of the MPD on the particle size indicated an advantage when carbon with small particle size was used as the fuel; however, it was difficult to wet very fine carbon particles of AC (70  $\mu\text{m}$ ) by molten carbonate to form a percolating carbonate phase at a lower ratio of carbonate:carbon (1:1).

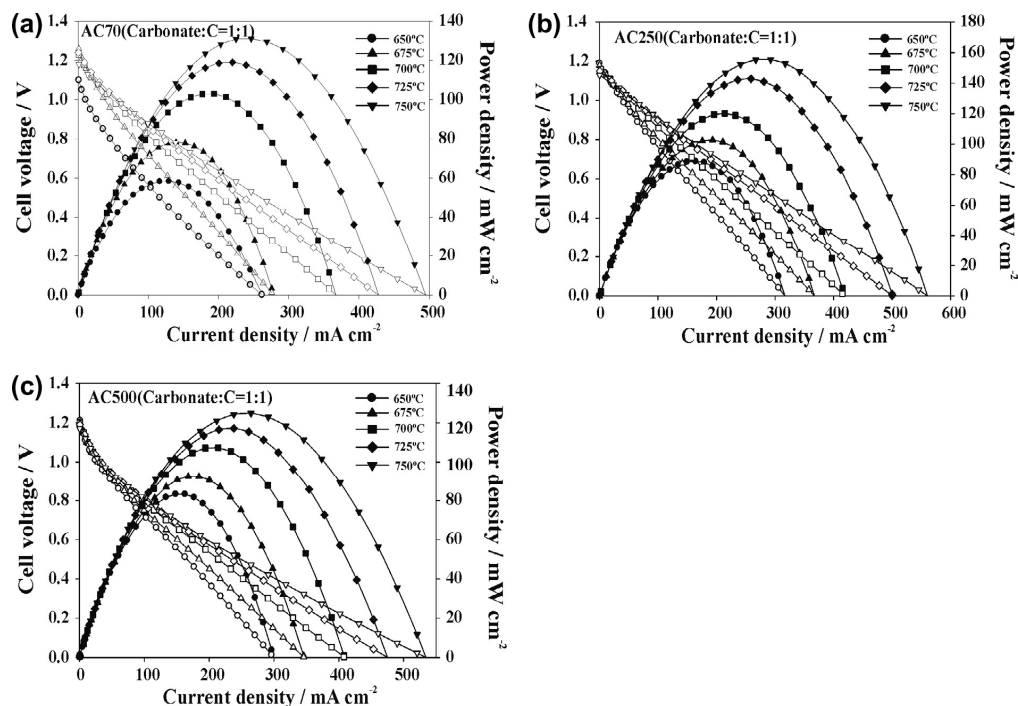
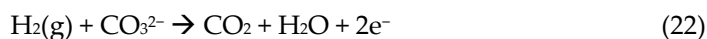


**Figure 9.** Different carbon fuel cell performances with different sizes of activated carbon fuels. Reproduced from Ref. [84], copyright 2013, with permission from Elsevier. (a) AC70; (b) AC250; (c) AC(500).

Anthracite and bituminous coals are promising candidates as the fuel for HDCFCs as they have a higher carbon content and higher conductivity than less ranked coals. The MPD of the HDCFC fueled with raw BiC was higher than that of raw AnC [90,93]. Short-term durability tests (<10 h) showed that the HDCFC fed with BiC had a slower performance drop than with AnC. Long-term duration tests for more than 120 h at 0.7 V, instead, showed a better performance of the AnC-fed HDCFC [93]. These results indicated that a high volatile matter, a high hydrogen content, and a low moisture content, as in the case of BiC, are desirable for a short-term operation, while for long-term operations, a high carbon content is preferable. To enhance the electrochemical performance of AnC and BiC, these carbons were submitted to pretreatments [90,104]. Thermal pretreatment of high-rank coals was not appropriate for their use in HDCFCs [90]. The air oxidation treatment, instead, can help to improve the reactivity of AnC coals (low H/C ratio). Oxidation pre-treatments can enhance some characteristics of AnC, such as oxygen content and reactivity. In the case of the BiC, instead, the formation of crosslinks and the reduction in aliphatic hydrogen during the oxidation pretreatment decrease the fluidity and the active area of the coal, leading to a lower cell performance. The pretreatment of BiC by pyrolysis at 800 °C, to remove organic volatiles, followed by modification with acetic acid, to reintroduce surface functional groups, increased cell performance [104]. Additional gas phase electrochemical reactions of  $\text{CO(g)}$  and  $\text{H}_2\text{(g)}$  released from the coals with  $\text{O}^{2-}$  and/or  $\text{CO}_3^{2-}$  ions can contribute to the OCV increase and electricity generation. Both oxidized AnC and BiC have certain oxygen functionalities, which will be released mainly as  $\text{CO(g)}$  during fuel cell operation, contributing to the CO mediator system via the electrochemical reaction (4). Regarding  $\text{H}_2\text{(g)}$ , part of the  $\text{H}_2$  can be involved in electrochemical reactions, according to reaction (21):



The electrochemical oxidation of  $\text{CO}(\text{g})$  and/or  $\text{H}_2(\text{g})$  released from the coals can also be promoted by carbonate ions present in the HDCFC, according to reactions (19) and (22):



### 3.3.6. Effect of Carbonate Mixture Composition

As can be seen in Table 2, apart from two works that report the use of an eutectic Li/Na carbonate composition, the eutectic Li/K carbonate mixture was used in HDCFCs. Cantero-Tubilla et al. [75] were the only ones to evaluate the effect of carbonate composition on the performance of an electrolyte-supported HDCFC. Alternative Li/K carbonate compositions (Li/Na, Li/Na/K, Li/Ba, and Na/K in eutectic compositions) were tested at the 6 vol% carbonate content. Sodium seems to have a negative effect on HDCFC performance. With Li/Na carbonates, the power density of the HDCFC decreased 50% and 30% at 700 and 800 °C, respectively, compared to that with Li/K carbonates. Potassium has a strong catalytic effect for carbon oxidation [138]. Lithium enhanced the catalytic activity of potassium, as shown by the comparison of the HDCFC performance with Li/K and Na/K carbonates: among all the compositions, the HDCFC with Na/K carbonate presented the lowest performance. Barium was also investigated as a replacement for Na and K ions. For temperatures >700 °C, the HDCFC with the Li/Ba carbonate eutectic showed a higher performance than that with Li/Na carbonates. Summarizing, the HDCFC with the Li/K carbonate eutectic showed the highest power density at all temperatures.

### 3.3.7. Effect of Catalyst Addition to the Fuel

A way to improve the performance of SO-DCFC is the addition of metal/metal oxide catalysts in the carbon fuel, enhancing the reverse Boudouard reaction to carry out the internal carbon gasification, providing more CO to the anode [139–145]. Ag, Ni, Co,  $\text{Ag}_2\text{O}$ ,  $\text{Fe}_2\text{O}_3$ , and CaO were the most used materials to catalyze the Boudouard reaction in SO-DCFCs. The addition of a catalyst to the carbon/carbonate fuel in HDCFCs was reported in some works [64,86,102]. The addition of 50 wt% Ni drastically improved the OCV, and in the full temperature range (550–900 °C), the MPD of the HDCFC was higher than that of the cell fueled with catalyst-free carbon [64].

The addition of silver-based catalysts to the carbon/carbonate slurry enhanced the performance of the HDCFC in the order  $\text{Ag} < \text{Ag}_2\text{CO}_3 < \text{Ag}_2\text{O}$  [86]. Kaklidis et al. [102] compared the performance of SO-DCFCs and HDCFCs, having the same cell structure, the only difference being the fuel composition, pure carbon, carbon/catalyst, carbon/carbonate, and catalyst/carbon/carbonate. A 20 wt% Co/CeO<sub>2</sub> catalyst was added to BiC fuel. An eutectic Li/K carbonate mixture was added to BiC and BiC/catalyst feedstock at a carbon/catalyst/carbonates weight ratio of 4:2:1, to evaluate the effect of catalyst and carbonates on cell performance. As it can be seen in Figure 10, where the histogram of the MPD at 800 °C of SO-DCFCs and HDCFCs, with and without catalyst in the fuel, is reported, the improvement in the cell fueled with the carbon/catalyst/carbonate mixture with respect to the cell fed with bare carbon is not the sum of carbonate and catalyst effects, but a synergic effect is clearly visible. The addition of carbonates facilitates BiC diffusion, while providing additional CO<sub>2</sub> through their thermal decomposition. The addition of catalyst improves the reverse Boudouard reaction and additional CO is produced, but its presence may interfere with the coal fluidity at the anode. The presence of catalyst and carbonates results in a beneficial effect on both the fluidity and the reverse Boudouard reaction, giving rise to higher power densities.

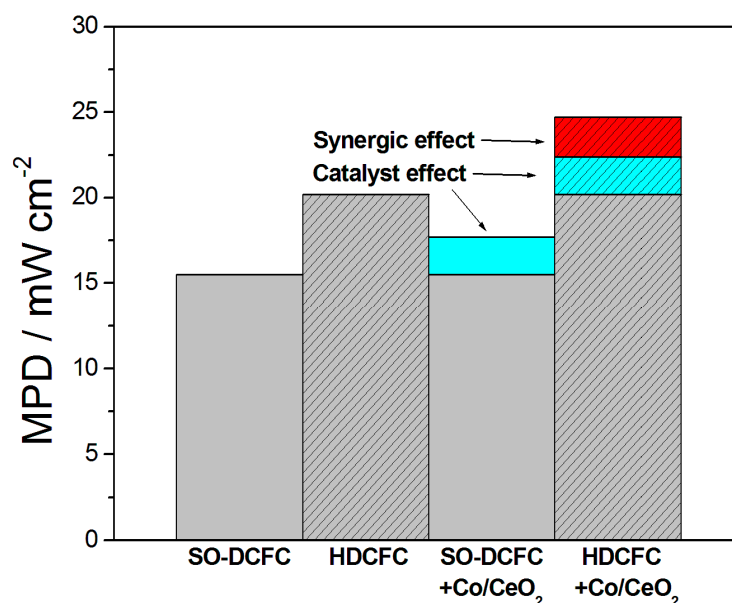


**Figure 10.** Histogram of the maximum power density (MPD) at 800 °C of solid oxide–direct carbon fuel cells (SO-DCFCs) and hybrid direct carbon fuel cells (HDCFCs), with and without catalyst in the fuel from data in Ref. [102].

### 3.3.8. Effect of Purge Gas

In DCFCs, an inert gas or CO<sub>2</sub> is often used to purge the reaction gas away from the TPB [4]. Purge gas significantly influences the OCV and cell performance. The presence of CO<sub>2</sub> enhances the reverse Boudouard reaction at temperatures >650 °C, giving rise to an improvement in cell performance, especially the MPD, by the electrochemical oxidation of formed CO [4]. Elleuch et al. [71] observed that the performance of an HDCFC depends on the nature of the purge gas and on temperature. Up to 700 °C, N<sub>2</sub> is preferred to keep the anode gas tight. Above 700 °C, as the reverse Boudouard reaction is thermodynamically favored, the performance of the cell with CO<sub>2</sub> as the purge gas was significantly higher than that with N<sub>2</sub>. The dependence of the ratio of the MPD with CO<sub>2</sub> purge gas to the MPD with N<sub>2</sub> purge gas (MPD<sub>CO2</sub>/MPD<sub>N2</sub>) on temperature and various types of fuels is shown in Figure 11a from data by Li et al. [96]. For all the fuels, the lower performance of the HDCFC in CO<sub>2</sub> flow than in N<sub>2</sub> flow at 650 °C is due to the increase in both ohmic and polarization resistances, the lower OCV, and, mainly, the poor kinetic of the reverse Boudouard reaction. For the HDCFCs fueled with AC and carbon black (BC), going from 650 to 700 °C, notwithstanding the lower OCV in CO<sub>2</sub> flow than in N<sub>2</sub> flow, the MPD<sub>CO2</sub>/MPD<sub>N2</sub> remarkably increased, due to the improved reverse Boudouard reaction. For the HDCFC fueled with GC, the improvement in the MPD<sub>CO2</sub>/MPD<sub>N2</sub> ratio was poor, since the stable structure of GC does not favor the reverse Boudouard reaction, and the microporous or nonporous structure in GC hindered the contact between carbon and molten carbonate. For all HDCFCs, by increasing the temperature from 700 to 750 °C, a slight decrease in the MPD<sub>CO2</sub>/MPD<sub>N2</sub> ratio was observed. At 750 °C in flowing N<sub>2</sub>, the enhanced carbonate decomposition (reaction 20) resulted in a higher amount of CO<sub>2</sub> formed, which generated more CO by the reverse Boudouard reaction. Conversely, in CO<sub>2</sub> flow, carbonate decomposition was hindered. The effect of carbonate amount in the fuel on the MPD<sub>CO2</sub>/MPD<sub>N2</sub> ratio is shown in Figure 11b from data in ref. 101. The addition of carbonates facilitated carbon diffusion and provided additional CO<sub>2</sub> through their thermal decomposition, generating CO by the reverse Boudouard reaction. By increasing the carbonate amount from 20 to 40 wt%, the improved carbon diffusion enhanced the reverse Boudouard reaction, thus explaining the higher MPD<sub>CO2</sub>/MPD<sub>N2</sub> ratio. In N<sub>2</sub> flow, a further increase in carbonate content in the fuel gave rise to more CO<sub>2</sub> formation by carbonate decomposition, increasing the reverse Boudouard reaction; this did not occur



in CO<sub>2</sub> flow, which prevented carbonate decomposition, making the use CO<sub>2</sub> purge gas less favorable and reducing the MPD<sub>CO2</sub>/MPD<sub>N2</sub> ratio.

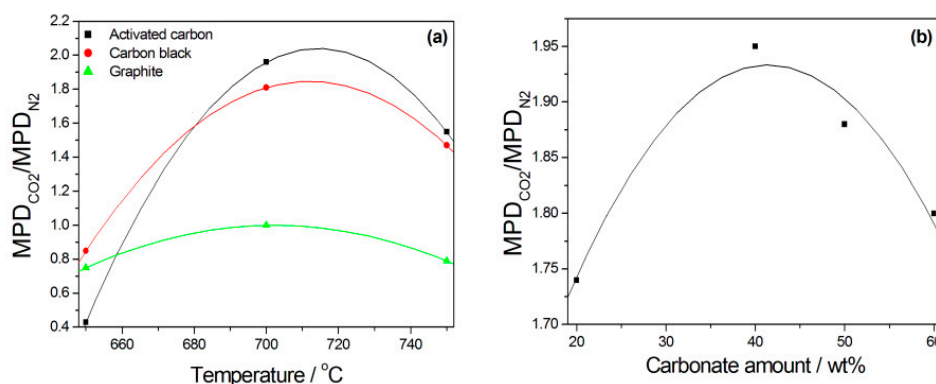


**Figure 11.** (a) Dependence of the ratio of the maximum power density (MPD) with CO<sub>2</sub> purge gas to the MPD with N<sub>2</sub> purge gas ( $MPD_{CO_2}/MPD_{N_2}$ ) on temperature and various types of fuels from data in Ref. [96]; (b) dependence of the  $MPD_{CO_2}/MPD_{N_2}$  ratio on carbonate amount in the fuel from data in Ref. [101].

### 3.3.9. Effect of Temperature

The dependence of the ratio of the  $x$  °C ( $T_x$ ) to 700 °C ( $T_0$ ) temperature maximum power density ( $MPD_{T_x}/MPD_{T_0}$ ) of HDCFCs on cell temperature from data in Table 2 is shown in Figure 12. As can be seen in Figure 8, as expected, in the temperature range of 650–900 °C, the  $MPD_{T_x}/MPD_{T_0}$  ratio almost linearly increases with temperature, independently of the catalyst and carbon type. An increase in temperature improves the electrochemical kinetics of both carbon oxidation and oxygen reduction reactions. Moreover, both carbon and oxygen transport diffusivities increase with increasing temperature, resulting in low mass transport.

An interesting way to improve HDCFC performance is size-matching between the carbon particles and anode pores. The optimal carbonate content also depends on the porosity and particle size of the carbon fuel: the higher the carbon surface area, the higher the amount of carbonate needed to wet the carbon surface.

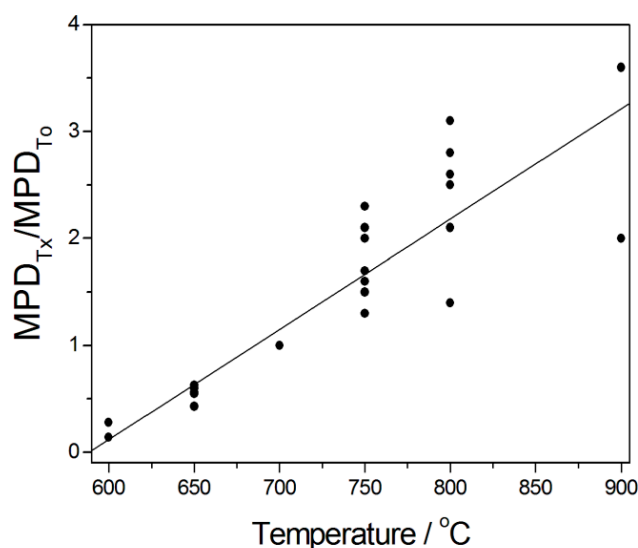
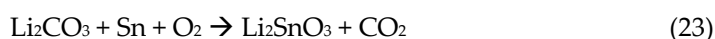


**Figure 12.** The dependence of the ratio of  $x$  °C ( $T_x$ ) to 700 °C ( $T_0$ ) temperature maximum power density ( $MPD_{T_x}/MPD_{T_0}$ ) of hybrid direct carbon fuel cells on cell temperature from data in Table 2.

#### 4. LTA-HDCFC and Liquid-tin-Containing HDCFC

Only two works addressed mixed molten metal/molten carbonate SO-DCFCs, one with LTA-HDCFC [146] and another with liquid-tin-containing-HDCFC [147]. Cao et al. [146] reported an LTA-HDCFC with a Sn-Li/K carbonate anode, an YSZ electrolyte, and a Pt cathode. With molten carbonate occupying the anode–electrolyte interface, the location of the Sn oxidation process changes from the anode–electrolyte interface to the carbonate–tin interface. Thus, the SnO<sub>2</sub> film formed on molten carbonate droplets is less stable than that formed on the solid electrolyte and can be reduced more easily. In the absence of carbon, that is, in battery mode, for a pure tin anode, a maximum current density of 581.7 A m<sup>−2</sup> was attained, followed by a sudden drop in current density, related to SnO<sub>2</sub> film formation. After carbonate addition, for the composite anode containing 2 mol.% carbonate, the maximum current density was 1068.9 A m<sup>−2</sup>, indicating that carbonate addition decreased the stability of the formed SnO<sub>2</sub> layer. To test the carbon conversion kinetics, the composite tin-carbonate anode was first discharged at 800 °C at a constant working potential of 0.4 V for 1 h, then 0.1 g of carbon black was introduced into the anode chamber. Before carbon introduction, the fuel cell performance reached its lowest value of 100.7 A m<sup>−2</sup>. Following carbon addition to the anode chamber, fuel cell performance increased abruptly to 208.6 A m<sup>−2</sup>. As solid carbon particles slowly migrated in the liquid metal anode, the immediate increase in fuel cell performance after fuel introduction was ascribed to the accelerated CO formation via Boudouard reaction in the presence of the molten carbonate. Then, a carbon-containing composite anode was prepared by adding 0.1 g of carbon black into the composite anode powder. The fuel cell with this carbon-containing anode was discharged at 800 °C at a constant working potential of 0.4 V. The performance of carbon mixed anode slightly decreased from 214.0 A m<sup>−2</sup> to 167.4 A m<sup>−2</sup> after the first 150 s. However, fuel cell performance increased in the later part of the discharge to a current density of 348.9 A m<sup>−2</sup> after 5000 s. At beginning of the discharge, Sn is consumed while the reduction rate of SnO<sub>2</sub> is relatively slow. In the later part of the discharge, SnO<sub>2</sub> is transported into the bulk of the anode and interacts with carbon. During the reduction of SnO<sub>2</sub> by carbon in the liquid phase anode, Sn metal is regenerated and CO is produced via the Boudouard reaction. By mixing carbon black homogeneously with the liquid anode, the escape of the CO is more difficult, resulting in an increased performance.

Li et al. [147] evaluated the effect of the addition of liquid Sn in various compositions (0, 10, 20, and 50 wt%) to Li/K carbonate on the performance of an anode-supported HDCFC, consisting of a Ni/YSZ anode, a thin YSZ electrolyte, and a GDC/LSCF composite cathode. At 750 °C, for the Sn-free anode, the MPD was, ca., 65 mW cm<sup>−2</sup>. When introducing molten Sn into the anode, the OCV does not change significantly, indicating that the OCV is related to the carbon and carbonates rather than Sn. In the presence of Sn, the MPD is dependent on the Sn concentration. The MPD values were 58, 86, and 49 mW cm<sup>−2</sup> for 10, 20, and 50 Sn wt% loading, respectively. Sn and Li<sub>2</sub>CO<sub>3</sub> can react to form a Li<sub>2</sub>SnO<sub>3</sub> phase:



As a consequence, the consumption of Sn and Li<sub>2</sub>CO<sub>3</sub> decreases the amount of oxidized carbon by Sn/SnO<sub>2</sub> and CO<sub>2</sub>/CO<sub>3</sub><sup>2−</sup> redox cycling reactions. Thus, the decrease in MPD for a high Sn content was ascribed to the formation of a large amount of Li<sub>2</sub>SnO<sub>3</sub>. When tuning the Sn amount to an optimal value (20 wt%), the catalytic reactions of both Sn-SnO<sub>2</sub> and Li-K systems prevail on the negative impact of Li<sub>2</sub>SnO<sub>3</sub> formation.

#### 5. Conclusions and Perspectives

LMA-DCFCs are an efficient tool for the direct electrochemical conversion of solid carbon into electrical energy. The first molten metals investigated acted only as physical mediators. In this case, their function is to enhance the carbon reaction active area by

changing the contact between the solid electrode and solid carbon into a liquid electrode and solid carbon. Carbon is oxidized by  $O^{2-}$  and the OCV is near 1 V. A physical mediator metal has to have a low affinity for oxygen and a high solubility of fuel and oxygen, its oxide has to be not stable at the cell operation temperature, and, if is stable, the metal oxide has to have poor reactivity with carbon. Cu and Ag are examples of physical mediator metals. A drawback of these metals, however, is their high melting temperature. Then, molten metals are used as physical and chemical mediators. When a molten metal acts as a chemical mediator, it is oxidized by  $O^{2-}$ , the OCV is less than 1 V, and its metal oxide has to be reduced by carbon spontaneously. Among different metals, only Sn and, overall, Sb are used as physical and chemical mediators. A serious drawback of LTA-SOFCs is the formation of an insulating  $SnO_2$  layer, so, generally, tin is not employed as a molten anode, but, mixed with carbon and in the presence of a solid anode, acts as an interfacial mediator. The only LMA-DCFC with an appreciable performance is Sb as the liquid anode. A critical issue of LAA-DCFCs is the corrosion of the electrolyte by liquid Sb/ $Sb_2O_3$  at operating cell temperatures. As electrolyte grain boundaries are weak points to Sb/ $Sb_2O_3$  attack, the reduction in their number can be a solution to resist corrosion. The ScSZ electrolyte prepared by APS technology presents a low number of grain boundaries, leading to a lower Sb migration and a higher electrolyte stability.  $Fe_2O_3$  is often used to form liquid phases at the grain boundaries during sintering processes and to improve grain-boundary conductivity [148]. The corrosion resistance of GDC electrolytes is enhanced by  $Fe_2O_3$  addition. Refined grains in  $Fe_2O_3$ -GDC with much longer and more tortuous grain boundaries would make the penetration of Sb/ $Sb_2O_3$  more difficult.

The introduction of carbonates in the SO-DCFC system leads to an enhancement of cell performance in terms of OCV and power output. The carbonates mainly act as a physical mediator, accelerating  $O^{2-}$  transfer to the anode TPB, but also as a chemical mediator for carbon oxidation reaction. Carbonates are almost effective at low temperatures and using poor performing fuels. The characteristics of carbon fuels play an important role in the performance of HDCFCs. Generally, a high surface area and a small particle size of carbon fuel can improve its electrochemical reactivity by increasing the interaction between the carbon particles and the anode catalyst. Conversely, a high graphitic degree of carbon fuel can lead to a lower electrochemical reactivity due to the less reactive sites on carbon surface. Moreover, the electrochemical reactivity of carbon fuels increases with increasing concentration of oxygen-containing functional groups on their surface. Carbon contaminants, in the form of ash, affect HDCFC performance, facilitating or hindering carbon electrooxidation, so it is fundamental to evaluate their role during cell operation. The highest HDCFC performance is obtained with coals containing high fixed carbon, low sulfur, and a medium amount of volatile material and moisture. To enhance their electrochemical performance, pretreatments, such as heat treatment, acid or base washing, and air oxidation, are carried out on carbon fuels. Pre-treatments, however, do not always lead to an improvement in performance, depending on carbon characteristics. To improve HDCFC performance, different ways have been suggested, either modifying the electrodes or optimizing the external parameters, such as carbon/carbonate ratio, purge gas, and operation mode. Appropriate doping of the perovskite anode (chemical modification) or increasing the catalyst surface area (physical modification) leads to an enhancement in cell performance. An interesting way to improve HDCFC performance is size-matching between the carbon particles and anode pores. The optimal carbonate content also depends on the porosity and particle size of the carbon fuel: the higher the carbon surface area, the higher the amount of carbonate needed to wet the carbon surface. The purge also influences cell performance. Up to 700 °C,  $N_2$  is the preferred purge gas to keep the anode gas tight. Above 700 °C, as the reverse Boudouard reaction is thermodynamically favored, the performance of the cell with  $CO_2$  as the purge gas is significantly higher than with  $N_2$ .

A serious drawback regarding HDCFCs is electrolyte corrosion by molten carbonates. YSZ is stable in reducing conditions, but not stable in oxidizing conditions. On the other hand, GDC is relatively stable in oxidizing conditions. Thus, a solution could be to use a composite double-layered YSZ/GDC electrolyte, with the YSZ layer at the anode side and the GDC layer at the cathode side. Another solution is to develop new carbonate corrosion-resistant materials, possessing suitable properties for their use as the electrolyte in HDCFCs, such as ionic conductivity and electronic insulation, good chemical compatibility with anode and cathode catalysts, and with the electrolyte TEC in close proximity to that of the electrode catalysts, to avoid cell cracking.

Finally, only two works addressed SO-DCFCs, with both molten tin and molten carbonates present in the anode chamber. As, in both studies, tin was used as the molten metal, there is plenty of room to explore this topic further in future works, in particular, using molten Sb.

**Funding:** This research received no external funding.

**Data Availability Statement:** No new data were created.

**Conflicts of Interest:** The author declares no conflict of interest.

### Abbreviations

Activated carbon, AC; anthracite coal, AnC; atmospheric plasma spray, APS; bituminous coal, BiC; demineralized bituminous coal, DBiC; direct carbon fuel cell, DCFC; hybrid direct carbon fuel cell, HDCFC; gadolinia-doped ceria, GDC; graphite, GC; lignite, PCF; liquid antimony anode–direct carbon fuel cell, LAA-DCFC; liquid metal anode–direct carbon fuel cell, LMA-DCFC; lanthanum strontium gallium magnesium oxide, LSGM; lanthanum strontium manganite, LSM; liquid tin anode–direct carbon fuel cell, LTA-DCFC; maximum power density, MPD; molten carbonate fuel cell, MCFC; open-circuit voltage, OCV; pine charcoal, PCC; samarium-doped ceria, SDC; scandia-stabilized zirconia, ScSZ; solid oxide–direct carbon fuel cell, SO-DCFC; solid oxide fuel cell, SOFC; thermal expansion coefficient, TEC; yttria-stabilized zirconia, YSZ.

### References

1. Gur, T.M. Critical review of carbon conversion in carbon fuel cells. *Chem. Rev.* **2013**, *113*, 6179–6206. <https://doi.org/10.1021/cr400072b>.
2. Giddey, S.; Badwal, S.P.S.; Kulkarni, A.; Munnings, C. A comprehensive review of direct carbon fuel cell technology. *Prog. Energy Combust. Sci.* **2012**, *38*, 360–399. <https://doi.org/10.1016/j.pecs.2012.01.003>.
3. Cao, D.; Sun, Y.; Wang, G. Direct carbon fuel cell: Fundamentals and recent developments. *J. Power Sources* **2007**, *167*, 250–257. <https://doi.org/10.1016/j.jpowsour.2007.02.034>.
4. Jiang, C.; Ma, J.; Corre, G.; Jain, S.L.; Irvine, J.T.S. Challenges in developing direct carbon fuel cells. *Chem. Soc. Rev.* **2017**, *46*, 2889–2912. <https://doi.org/10.1039/C6CS00784H>.
5. Yu, F.; Han, T.; Wang, Z.; Xie, Y.; Wu, Y.; Jin, Y.; Yang, N.; Xiao, J.; Kawi, S. Recent progress in direct carbon solid oxide fuel cell: Advanced anode catalysts, diversified carbon fuels, and heat management. *Int. J. Hydrogen Energy* **2021**, *46*, 4283–4300. <https://doi.org/10.1016/j.ijhydene.2020.10.259>.
6. Deleebeeck, L.; Hansen, K.K. Hybrid direct carbon fuel cells and their reaction mechanisms—a review. *J. Solid State Electrochem.* **2014**, *18*, 861–882. <https://doi.org/10.1007/s10008-013-2258-1>.
7. Jewulski, J.; Skrzypkiewicz, M. Direct carbon fuel cells based on solid oxide electrolyte technology. *Prz. Elektrotechniczny* **2013**, *89*, 268–270.
8. Toleuova, A.; Yufit, V.; Simons, S.; Maskell, W.C.; Brett, D.J.L. A review of liquid metal anode solid oxide fuel cells. *J. Electrochem. Sci. Eng.* **2013**, *3*, 91–105. <https://doi.org/10.5599/jese.2013.0032>.
9. Abernathy, H.; Gemmen, R.; Gerdes, K.; Koslowske, M.; Tao, T. Basic properties of a liquid tin anode solid oxide fuel cell. *J. Power Sources* **2011**, *196*, 4564–4572. <https://doi.org/10.1016/j.jpowsour.2010.12.089>.
10. Tao, T.; Bateman, L.; Bentley, J.; Slaney, M. Liquid tin anode solid oxide fuel cell for direct carbonaceous fuel conversion. *ECS Trans.* **2007**, *5*, 463–472. <https://doi.org/10.1149/1.2729026>.
11. Yentekakis, I.V.; Debenedetti, P.G.; Costa, B. Novel fused metal anode solid electrolyte fuel cell for direct coal gasification: A steady-state model. *Ind. Eng. Chem. Res.* **1989**, *28*, 1414–1424. <https://doi.org/10.1021/ie00093a022>.

12. Yentekakis, I.V.; Debenedetti, P.G.; Costa, B.; Konsolakis, M.; Kiouisis, V. Direct coal gasification with simultaneous production of electricity in a novel fused metal anode SOFC: A theoretical approach. *Ionics* **1999**, *5*, 460–471. <https://doi.org/10.1007/BF02376014>.
13. Jayakumar, A.; Javadekar, A.; Gissinger, J.; Vohs, J.M.; Huber, G.W.; Gorte, R.J. The stability of direct carbon fuel cells with molten Sb and Sb-Bi alloy anodes. *AIChE J.* **2013**, *59*, 3342–3348. <https://doi.org/10.1002/aic.13965>.
14. Gur, T.M. Direct Carbon Fuel Cell with Molten Anode. U.S. Patent n. 2006/023409, 19 October 2006.
15. Jacobs, K.T. A new type of SOFC for conversion of high temperature heat to electricity without Carnot limitation. *ECS Trans.* **2011**, *35*, 573–582. <https://doi.org/10.1149/1.3570035>.
16. Javadekar, A.; Jayakumar, A.; Pujara, R.; Vohs, J.M.; Gorte, R.J. Molten silver as a direct carbon fuel cell anode. *J. Power Sources* **2012**, *214*, 239–243. <https://doi.org/10.1016/j.jpowsour.2012.04.096>.
17. Jayakumar, A.; Hornés, A.; Vohs, J.M.; Gorte, R.J. A comparison of molten Sn and Bi for solid oxide fuel cell anodes. *J. Electrochem. Soc.* **2010**, *157*, B365–B369. <https://doi.org/10.1149/1.3282443>.
18. Jayakumar, A.; Vohs, J.M.; Gorte, R.J. Molten-metal electrodes for solid oxide fuel cells. *Ind. Eng. Chem. Res.* **2010**, *49*, 10237–10241. <https://doi.org/10.1021/ie100457t>.
19. Duan, N.-Q.; Cao, Y.; Hua, B.; Chi, B.; Pu, J.; Luo, J.; Jian, L. Tubular direct carbon solid oxide fuel cells with molten antimony anode and refueling feasibility. *Energy* **2016**, *95*, 274–278. <https://doi.org/10.1016/j.energy.2015.10.033>.
20. Cao, T.; Wang, H.; Shi, Y.; Cai, N. Direct carbon fuel conversion in a liquid antimony anode solid oxide fuel cell. *Fuel* **2014**, *135*, 223–227. <https://doi.org/10.1016/j.fuel.2014.07.007>.
21. Jayakumar, A. Molten Metal Anodes for Direct Carbon-Solid Oxide Fuel Cells. Publicly Accessible Penn Dissertations. 646, 2012. Available online: <https://repository.upenn.edu/edissertations/646> (accessed on 2 March 2023).
22. Kim, B.-S.; Lee, J.; Yoon, H.S.; Kim, S.-K. Reduction of SnO<sub>2</sub> with hydrogen. *Mater. Trans.* **2011**, *52*, 1814–1817. <https://doi.org/10.2320/matertrans.M2011118>.
23. Wang, H.; Shi, Y.; Cai, N. Characteristics of liquid stannum anode fuel cell operated in battery mode and CO/H<sub>2</sub>/carbon fuel mode. *J. Power Sources* **2014**, *246*, 204–212. <https://doi.org/10.1016/j.jpowsour.2013.07.085>.
24. Tao, T.; Slaney, M.; Bateman, L.; Bentley, J.J. Anode polarization in liquid tin anode solid oxide fuel cell. *ECS Trans.* **2007**, *7*, 1389–1397. <https://doi.org/10.1149/1.2729243>.
25. Rastler, D. *Program on Technology Innovation: Systems Assessment of Direct Carbon Fuel Cells Technology*, Electric Power Research Report; Number 1016170; EPRI: Alto, CA, USA, 14 May 2008.
26. Jayakumar, A.; Kungas, R.; Roy, S.; Javadekar, A.; Buttrey, D.J.; Vohs, J.M.; R.J.; Gorte, R.J. A direct carbon fuel cell with a molten antimony anode. *Energy Environ. Sci.* **2011**, *4*, 4133–4137. <https://doi.org/10.1039/C1EE01863A>.
27. Ju, H.K.; Uhm, S.; Kim, J.W.; Song, R.-H.; Choi, H.; Lee, S.-H.; Lee, J. Enhanced anode interface for electrochemical oxidation of solid fuel in direct carbon fuel cells: The role of liquid Sn in mixed state. *J. Power Sources* **2012**, *198*, 36–41. <https://doi.org/10.1016/j.jpowsour.2011.09.082>.
28. Xu, X.; Zhou, W.; Zhu, Z. Samaria-doped ceria electrolyte supported direct carbon fuel cell with molten antimony as the anode. *Ind. Eng. Chem. Res.* **2013**, *52*, 17927–17933. <https://doi.org/10.1021/ie403164c>.
29. Wang, H.; Cao, T.; Shi, Y.; Cai, N.; Yuan, W. Liquid antimony anode direct carbon fuel cell fueled with mass-produced de-ash coal. *Energy* **2014**, *75*, 555–559. <https://doi.org/10.1016/j.energy.2014.08.017>.
30. Khurana, S.; LaBarbera, M.; Fedkin, M.V.; Lvov, S.N.; Abernathy, H.; Gerdes, K. Performance evaluation of a liquid tin anode solid oxide fuel cell operating under hydrogen, argon and coal, *J. Power Sources* **2015**, *274*, 1049–1054. <https://doi.org/10.1016/j.jpowsour.2014.10.138>.
31. Duan, N.-Q.; Tan, Y.; Yan, D.; Jia, L.; Chi, B.; Pu, J.; Jian, L. Biomass carbon fueled tubular solid oxide fuel cells with molten antimony anode. *Appl. Energy* **2016**, *165*, 983–989. <https://doi.org/10.1016/j.apenergy.2015.11.050>.
32. Jang, H.; Eom, J.; Ju, H.K.; Lee, J. Ameliorated performance in a direct carbon fuel cell using Sn mediator on Ni-YSZ anode surface. *Catal. Today* **2016**, *260*, 158–164. <https://doi.org/10.1016/j.cattod.2015.06.013>.
33. Xu, K.; Li, Z.; Shi, M.; Xing, H.; Liu, H.; Li, X.; Hu, H.; Luo, G.; Yao, H. Investigation of the anode reactions in SO-DCFCs fueled by Sn–C mixture fuels. *Proc. Comb. Inst.* **2017**, *36*, 4435–4442. <https://doi.org/10.1016/j.proci.2016.06.171>.
34. Duan, N.; Xue, Y.; Ma, J.; Han, Y.; Xu, M.; Chi, B.; Pu, J.; Li, J. Liquid antimony-silver alloys as anodes for direct carbon solid oxide fuel cells. *J. Power Sources* **2018**, *397*, 170–176. <https://doi.org/10.1016/j.jpowsour.2018.07.011>.
35. Cao, T.; Song, P.; Shi, Y.; Ghoniem, A.F.; Cai, N. Oxy-combustion of coal in liquid-antimony-anode solid oxide fuel cell system. *Proc. Comb. Inst.* **2019**, *37*, 2841–2848. <https://doi.org/10.1016/j.proci.2018.08.056>.
36. Levêque, G.; Abanades, S. Thermodynamic and kinetic study of the carbothermal reduction of SnO<sub>2</sub> for solar thermochemical fuel generation. *Energy Fuels* **2014**, *28*, 1396–1405. <https://doi.org/10.1021/ef402182g>.
37. Zhou, X.; Oh, T.-S.; Vohs, J.M.; Gorte, R.J. Zirconia-based electrolyte stability in direct-carbon fuel cells with molten Sb anodes. *J. Electrochem. Soc.* **2015**, *162*, F567–F570. <https://doi.org/10.1149/2.0871506jes>.
38. Cao, T.; Cheng, Y.; Gorte, R.J.; Shi, Y.; Vohs, J.M.; Cai, N. Effect of grain boundary diffusion on electrolyte stability in direct carbon fuel cells with antimony anodes. *Ceram. Int.* **2017**, *43*, 16575–16579. <https://doi.org/10.1016/j.ceramint.2017.09.045>.

39. Ma, J.; Duan, N.; Han, Y.; Yan, D.; Chi, B.; Pu, J.; Li, J. Hot corrosion of Gd<sub>2</sub>O<sub>3</sub>-doped CeO<sub>2</sub> electrolyte in solid oxide fuel cells with a liquid antimony anode. *J. Power Sources* **2018**, *401*, 397–402. <https://doi.org/10.1016/j.jpowsour.2018.08.083>.
40. Ma, J.; Duan, N.; Han, Y.; Li, P.; Zhu, B.; Yan, D.; Chi, B.; Pu, J.; Li, J. Hot corrosion of yttria-stabilized zirconia by liquid antimony and antimony oxide. *J. Power Sources* **2019**, *434*, 226764. <https://doi.org/10.1016/j.jpowsour.2019.226764>.
41. Cao, T.; Huang, K.; Shia, Y.; Cai, N. Plasma-spray derived, corrosion-resistive electrolyte for liquid antimony anode direct carbon fuel cell. *J. Power Sources* **2018**, *403*, 76–81. <https://doi.org/10.1016/j.jpowsour.2018.09.036>.
42. Singh, H.; Sidhu, B.S.; Puri, D.; Prakash, S. Use of plasma spray technology for deposition of high temperature oxidation/corrosion resistant coatings—a review. *Mater. Corros.* **2007**, *58*, 92–102. <https://doi.org/10.1002/maco.200603985>.
43. Han, Y.; Ma, J.; Duan, N.; Yang, J.; Yan, D.; Chi, B.; Pu, J.; Li, J. Enhanced resistance of gadolinium-doped cerium oxide to liquid antimony and antimony oxide corrosions by addition of iron oxide. *J. Power Sources* **2020**, *455*, 227970. <https://doi.org/10.1016/j.jpowsour.2020.227970>.
44. Jacques, W.W. *Harper's New Monthly Magazine*. V.94 1896–1897; 1987; pp. 144–150. Harper & Brothers, New York, NY.
45. Zecevic, S.; Patton, E.M.; Parharni, P. Carbon-air fuel cell without a reforming process. *Carbon* **2004**, *42*, 1983–1993. <https://doi.org/10.1016/j.carbon.2004.03.036>.
46. Guo, L.; Calo, J.M.; DiCocco, E.; Bain, E.J. Development of a low temperature, molten hydroxide direct carbon fuel cell. *Energy Fuels* **2013**, *27*, 1712–1719. <https://doi.org/10.1021/ef302100h>.
47. Guo, L.; Calo, J.M.; Kearney, C.; Grimshaw, P. The anodic reaction zone and performance of different carbonaceous fuels in a batch molten hydroxide direct carbon fuel cell. *Appl. Energy* **2014**, *129*, 32–38. <https://doi.org/10.1016/j.apenergy.2014.05.005>.
48. Kacprzak, A.; Kobylecki, R.; Bis, Z. The effect of coal thermal pretreatment on the electrochemical performance of molten hydroxide direct carbon fuel cell (MH-DCFC). *J. Power Tech.* **2017**, *97*, 382–387.
49. Weaver, E.D.; Leach, S.C.; Bayce, A.F.; Nanis, L. Direct electrochemical generation of electricity from coal. *SRI* **1976**, *97*, 382–387, Menlo Park CA 94025 SAN.
50. Antolini, E. The stability of molten carbonate fuel cell electrodes: A review of recent improvements. *Appl. Energy* **2011**, *88*, 4274–4293. <https://doi.org/10.1016/j.apenergy.2011.07.009>.
51. Kouchachvili, L.; Ikura, M. Performance of direct carbon fuel cell. *Int. J. Hydrogen Energy* **2011**, *36*, 10263–10268. <https://doi.org/10.1016/j.ijhydene.2010.10.036>.
52. Cherepy, N.J.; Krueger, R.; Fiet, K.J.; Jankowski, A.F.; Cooper, J.F. Direct conversion of carbon fuels in a molten carbonate fuel cell. *J. Electrochem. Soc.* **2005**, *152*, A80–A87. <https://doi.org/10.1149/1.1836129>.
53. Chen, M.; Wang, C.; Niu, X.; Xhao, S.; Tang, J.; Zhu, B. Carbon anode in direct carbon fuel cell. *Int. J. Hydrogen Energy* **2010**, *35*, 2732–2736. <https://doi.org/10.1016/j.ijhydene.2009.04.051>.
54. Vutetakis, D.G.; Skidmore, D.R.; Byker, H.J. Electrochemical oxidation of molten carbonate-coal slurries. *J. Electrochem. Soc.* **1987**, *134*, 3027–3034. <https://doi.org/10.1149/1.2100334>.
55. Ido, A.; Kawase, M. Development of a tubular molten carbonate direct carbon fuel cell and basic cell performance. *J. Power Sources* **2020**, *449*, 227483. <https://doi.org/10.1016/j.jpowsour.2019.227483>.
56. Cui, C.; Li, S.; Gong, J.; Wei, K.; Hou, X.; Jiang, C.; Yao, Y.; Ma, J. Review of molten carbonate-based direct carbon fuel cells. *Mater. Renew. Sust. Energy* **2021**, *10*, 12. <https://doi.org/10.1007/s40243-021-00197-7>.
57. Metcalfe, C.; Kesle, O. Influence of microstructure on electrochemical performance of plasma sprayed Ni-YSZ anodes for SOFCs. *Fuel Cells* **2020**, *20*, 730–740. <https://doi.org/10.1002/fuce.201900233>.
58. Liu, C.; Pu, J.; Chen, X.; Ma, Z.; Ding, X.; Zhou, J.; Wang, S. Influence of anode's microstructure on electrochemical performance of solid oxide direct carbon fuel cells. *Int. J. Hydrogen Energy* **2020**, *46*, 11784–11790. <https://doi.org/10.1016/j.ijhydene.2020.02.119>.
59. Peelen, W.H.A.; Hemmes, K.; de Wit, J.H.W. Carbon a major energy carrier for the future? Direct carbon fuel cells and molten salt coal/biomass gasification. *High Temp. Mater. Proc.* **1998**, *2*, 471–482.
60. Bonaccorso, A.D.; Irvine, J.T.S. Development of tubular hybrid direct carbon fuel cell. *Int. J. Hydrogen Energy* **2012**, *37*, 19337–19344. <https://doi.org/10.1016/j.ijhydene.2012.02.104>.
61. Xie, H.; Zhai, S.; Liu, T.; Liao, H.; Zhang, Y.; Zhou, W.; Shao, Z.; Ni, M.; Chen, B. Cu-modified Ni foams as three-dimensional outer anodes for high-performance hybrid direct coal fuel cells. *Chem. Eng. J.* **2021**, *410*, 128239. <https://doi.org/10.1016/j.cej.2020.128239>.
62. Nabae, Y.; Pointon, K.D.; Irvine, J.T.S. Electrochemical oxidation of solid carbon in hybrid DCFC with solid oxide and molten carbonate binary electrolyte. *Energy Environ. Sci.* **2008**, *1*, 148–155. <https://doi.org/10.1039/B804785E>.
63. White, S.H.; Twardoch, U.M. The solubility and electrochemistry of alkali metal oxides in the molten eutectic mixture of lithium carbonate-sodium carbonate-potassium carbonate. *J. Appl. Electrochem.* **1989**, *19*, 901–910. <https://doi.org/10.1007/BF01007939>.
64. Nabae, Y.; Pointon, K.D.; Irvine, J.T.S. Ni/C slurries based on molten carbonates as a fuel for hybrid direct carbon fuel cells. *J. Electrochem. Soc.* **2009**, *156*, B716–B720. <https://doi.org/10.1149/1.3110862>.
65. Jiang, C.; Irvine, J.T.S. Catalysis and oxidation of carbon in a hybrid direct carbon fuel cell. *J. Power Sources* **2011**, *196*, 7318–7322. <https://doi.org/10.1016/j.jpowsour.2010.11.066>.

66. Chien, A.C.; Irvine, J.T.S. Hybrid molten carbonate/solid oxide direct carbon fuel cells. In *Molten Salts Chemistry, From Lab to Applications*; Lantelme, F., Groult, H., Eds.; 2013; Chapter 19, pp. 403–414. Elsevier. <https://doi.org/10.1016/B978-0-12-398538-5.00019-6>.
67. Badwal, S.; Giddey, S. The holy grail of carbon combustion—The Direct Carbon Fuel Cell technology. *Mater. Forum* **2010**, *34*, 181–185. <http://hdl.handle.net/102.100.100/105843?index=1>.
68. Lipilin, A.S.; Balachov, I.I.; Dubois, L.H.; Sanjurjo, A.; McKubre, M.C.; Crouch-Baker, S.; Hornbostel, M.D.; Tanzella, F.L. Liquid Anode Electrochemical Cell. U.S. Patent 2007/0269688 A1, 2007.
69. Cooper, J.F.; Direct conversion of coal derived carbon in fuel cell, In Basu S. (Eds.) Recent trends in fuel cell science and technology, Springer, New York, NY. [https://doi.org/10.1007/978-0-387-68815-2\\_10](https://doi.org/10.1007/978-0-387-68815-2_10).
70. Jia, L.; Tian, Y.; Liu, Q.; Xia, C.; Yu, J.; Wang, Z.; Zhao, Y.; Li, Y. A direct carbon fuel cell with (molten carbonate)/(doped ceria) composite electrolyte. *J. Power Sources* **2010**, *195*, 5581–5586. <https://doi.org/10.1016/j.jpowsour.2010.03.016>.
71. Elleuch, A.; Yu, J.; Boussetta, A.; Halouani, K.; Li, Y. Electrochemical oxidation of graphite in an intermediate temperature direct carbon fuel cell based on two-phases electrolyte. *Int. J. Hydrogen Energy* **2013**, *38*, 8514–8523. <https://doi.org/10.1016/j.ijhydene.2012.11.070>.
72. Elleuch, A.; Boussetta, A.; Yu, J.; Halouani, K.; Li, Y. Experimental investigation of direct carbon fuel cell fueled by almond shell biochar: Part I. Physico-chemical characterization of the biochar fuel and cell performance examination. *Int. J. Hydrogen Energy* **2013**, *38*, 16590–16604. <https://doi.org/10.1016/j.ijhydene.2013.08.090>.
73. Elleuch, A.; Halouani, K.; Li, Y. Investigation of chemical and electrochemical reactions mechanisms in a direct carbon fuel cell using olive wood charcoal as sustainable fuel. *J. Power Sources* **2015**, *281*, 350–361. <https://doi.org/10.1016/j.jpowsour.2015.01.171>.
74. Elleuch, A.; Boussetta, A.; Halouani, K.; Li, Y. Experimental investigation of direct carbon fuel cell fueled by almond shell biochar: Part II. Improvement of cell stability and performance by a three-layer planar configuration. *Int. J. Hydrogen Energy* **2013**, *38*, 16605–16614. <https://doi.org/10.1016/j.ijhydene.2013.07.061>.
75. Cantero-Tubilla, B.; Xu, C.; Zondlo, J.W.; Sabolsky, K.; Sabolsky, E.M. Investigation of anode configurations and fuel mixtures on the performance of direct carbon fuel cells (DCFCs). *J. Power Sources* **2013**, *238*, 227–235. <https://doi.org/10.1016/j.jpowsour.2013.03.072>.
76. Xu, X.; Zhou, W.; Liang, F.; Zhu, Z. Optimization of a direct carbon fuel cell for operation below 700 °C. *Int. J. Hydrogen Energy* **2013**, *38*, 5367–5374. <https://doi.org/10.1016/j.ijhydene.2013.02.066>.
77. Kakkidis, N.; Kyriakou, V.; Garagounis, I.; Arenillas, A.; Menendez, J.A.; Marnellos, G.E.; Konsolakis, M. Effect of carbon type on the performance of a direct or hybrid carbon solid oxide fuel cell. *RSC Adv.* **2014**, *4*, 18792–18800. <https://doi.org/10.1039/C4RA01022A>.
78. Kemm, M.; Stiller, C.; Selimovic, A.; Thorud, B.; Torisson, T.; Bolland, O. Planar and tubular solid oxide fuel cells: A comparison of transient process behaviors, *ECS Proc.* **2005**, 2005–2007, 659. <https://doi.org/10.1149/200507.0659PV>.
79. Baharuddin, N.A.; Muchtar, A.; Sulong, A.B.; Abdullah, H. Fabrication methods for planar solid oxide fuel cells: A review. *Adv. Mater. Res.* **2013**, *662*, 396–401. <https://doi.org/10.4028/www.scientific.net/AMR.662.396>.
80. Khan, M.Z.; Iltaf, A.; Ishfaq, H.A.; Khan, F.N.; Tanveer, W.H.; Song, R.-H.; Mehran, M.T.; Saleem, M.; Hussain, A.; Masaud, Z. Flat-tubular solid oxide fuel cells and stacks: A Review. *J. Asian Ceram. Soc.* **2021**, *9*, 745–770. <https://doi.org/10.1080/21870764.2021.1920135>.
81. Gil, V.; Gurauskis, J.; Deleebeeck, L.; Stamate, E.; Hansen, K.K. Cathode-supported hybrid direct carbon fuel cells. *Int. J. Hydrogen Energy* **2017**, *42*, 4311–4319. <https://doi.org/10.1016/j.ijhydene.2016.11.049>.
82. Pointon, K.; Lakemana, B.; Irvine, J.; Bradley, J.; Jain, S. The development of a carbon–air semi fuel cell. *J. Power Sources* **2006**, *162*, 750–756. <https://doi.org/10.1016/j.jpowsour.2005.07.023>.
83. Jiang, C.; Ma, J.; Bonaccorso, A.D.; Irvine, J.T.S. Demonstration of high power, direct conversion of waste-derived carbon in a hybrid direct carbon fuel cell. *Energy Environ. Sci.* **2012**, *5*, 6973–6980. <https://doi.org/10.1039/C2EE03510C>.
84. Xu, X.; Zhou, W.; Liang, F.; Zhu, Z. A comparative study of different carbon fuels in an electrolyte-supported hybrid direct carbon fuel cell. *Appl. Energy* **2013**, *108*, 402–409. <https://doi.org/10.1016/j.apenergy.2013.03.053>.
85. Chien, A.C.; Corre, G.; Antunes, R.; Irvine, J.T.S. Scaling up of the hybrid direct carbon fuel cell technology. *Int. J. Hydrogen Energy* **2013**, *38*, 8497–8502. <https://doi.org/10.1016/j.ijhydene.2012.10.097>.
86. Deleebeeck, L.; Ippolito, D.; Hansen, K.K. Enhancing Hybrid Direct Carbon Fuel Cell anode performance using Ag<sub>2</sub>O. *Electrochim. Acta* **2015**, *152*, 222–223. <https://doi.org/10.1016/j.electacta.2014.11.064>.
87. Chien, A.C.; Arenillas, A.; Jiang, C.; Irvine, J.T.S. Performance of direct carbon fuel cells operated on coal and effect of operation mode. *J. Electrochem. Soc.* **2014**, *161*, F588–F593. <https://doi.org/10.1149/2.925405jes>.
88. Lee, J.-Y.; Song, R.-H.; Lee, S.-B.; Lim, T.-H.; Park, S.-J.; Shul, Y.G.; Lee, J.-W. A performance study of hybrid direct carbon fuel cells: Impact of anode microstructure. *Int. J. Hydrogen Energy* **2014**, *39*, 11749–11755. <https://doi.org/10.1016/j.ijhydene.2014.05.145>.
89. Yu, J.; Zhao, Y.; Li, Y. Utilization of corn cob biochar in a direct carbon fuel cell. *J. Power Sources* **2014**, *270*, 312–317. <https://doi.org/10.1016/j.jpowsour.2014.07.125>.



90. Fuente-Cuesta, A.; Jiang, C.; Arenillas, A.; Irvine, J.T.S. Role of coal characteristics in the electrochemical behavior of hybrid direct carbon fuel cells. *Energy Environ. Sci.* **2016**, *9*, 2868–2880. <https://doi.org/10.1039/C6EE01461E>.
91. Cantero-Tubilla, B.; Sabolsky, K.; Sabolsky, E.M.; Zondlo, J.W. Investigation of pretreated switchgrass, corn stover, and hardwood fuels in direct carbon fuel cells. *Int. J. Electrochem. Sci.* **2016**, *11*, 303–321.
92. Hao, W.; Mi, Y. Evaluation of waste paper as a source of carbon fuel for hybrid direct carbon fuel cells. *Energy* **2016**, *107*, 122–130. <https://doi.org/10.1016/j.energy.2016.04.012>.
93. Jiang, C.; Ma, J.; Arenillas, A.; Bonaccorso, A.D.; Irvine, J.T.S. Comparative study of durability of hybrid direct carbon fuel cells with anthracite coal and bituminous coal. *Int. J. Hydrogen Energy* **2016**, *41*, 18797–18806. <https://doi.org/10.1016/j.ijhydene.2016.04.047>.
94. Yue, X.; Arenillas, A.; Irvine, J.T.S. Application of infiltrated LSCM-GDC oxide anode in direct carbon/coal fuel cells. *Faraday Discuss.* **2016**, *190*, 269–289. <https://doi.org/10.1039/C6FD00001K>.
95. Kaklidis, N.; Kyriakou, V.; Marnellos, G.E.; Strandbakke, R.; Arenillas, A.; Menéndez, J.A.; Konsolakis, M. Effect of fuel thermal pretreatment on the electrochemical performance of a direct lignite coal fuel cell. *Solid State Ion.* **2016**, *288*, 140–146. <https://doi.org/10.1016/j.ssi.2015.12.003>.
96. Li, S.; Pan, W.; Wang, S.; Meng, X.; Jiang, C.; Irvine, J.T.S. Electrochemical performance of different carbon fuels on a hybrid direct carbon fuel cell. *Int. J. Hydrogen Energy* **2017**, *42*, 16279–16287. <https://doi.org/10.1016/j.ijhydene.2017.05.150>.
97. Sun, K.; Liu, J.; Feng, J.; Yuan, H.; He, M.; Xu, C.; Wang, Z.; Sun, W.; Qiao, J. Investigation of B-site doped perovskites  $\text{Sr}_2\text{Fe}_{1.4}\text{X}_{0.1}\text{Mo}_{0.5}\text{O}_{6-\delta}$  (X=Bi, Al, Mg) as high-performance anodes for hybrid direct carbon fuel cell. *J. Power Sources* **2017**, *365*, 109–116. <https://doi.org/10.1016/j.jpowsour.2017.08.083>.
98. Wu, W.; Zhang, Y.; Ding, D.; He, T. A high-performing direct carbon fuel cell with a 3D architected anode operated below 600 °C. *Adv. Mater.* **2018**, *30*, 1704745. <https://doi.org/10.1002/adma.201704745>.
99. Liu, J.; Qiao, J.; Yuan, H.; Feng, J.; Sui, C.; Wang, Z.; Sun, W.; Sun, K. Ni modified  $\text{Ce}(\text{Mn}, \text{Fe})\text{O}_2$  cermet anode for high-performance direct carbon fuel cell. *Electrochim. Acta* **2017**, *232*, 174–181. <https://doi.org/10.1016/j.electacta.2017.02.135>.
100. Liu, J.; Yuan, H.; Qiao, J.; Feng, J.; Xu, C.; Wang, Z.; Sun, W.; Sun, K. Hierarchical hollow nanofiber networks for high-performance hybrid direct carbon fuel cells. *J. Mater. Chem. A* **2017**, *5*, 17216–17220. <https://doi.org/10.1039/C7TA04616B>.
101. Li, S.; Jiang, C.; Liu, J.; Tao, H.; Meng, X.; Connor, P.; Hui, J.; Wang, S.; Ma, J.; Irvine, J.T.S. Mechanism of enhanced performance on a hybrid direct carbon fuel cell using sawdust biofuels. *J. Power Sources* **2018**, *383*, 10–16. <https://doi.org/10.1016/j.jpowsour.2018.02.040>.
102. Kaklidis, N.; Strandbakke, R.; Arenillas, A.; Menendez, J.A.; Konsolakis, M.; Marnellos, G.E. The synergistic catalyst-carbonates effect on the direct bituminous coal fuel cell performance. *Int. J. Hydrogen Energy* **2019**, *44*, 10033–10042. <https://doi.org/10.1016/j.ijhydene.2019.02.038>.
103. Jiang, C.; Cui, C.; Ma, J.; Irvine, J.T.S. Insight into graphite oxidation in a NiO-based hybrid direct carbon fuel cell. *Int. J. Hydrogen Energy* **2020**, *45*, 10559–10568. <https://doi.org/10.1016/j.ijhydene.2019.08.208>.
104. Xie, H.; Zhai, S.; Chen, B.; Liu, T.; Zhang, Y.; Ni, M.; Shao, Z. Coal pretreatment and Ag-infiltrated anode for high-performance hybrid direct coal fuel cell. *Appl. Energy* **2020**, *260*, 114197. <https://doi.org/10.1016/j.apenergy.2019.114197>.
105. Ma, M.; Qiao, J.; Yang, X.; Xu, C.; Ren, R.; Sun, W.; Sun, K.; Wang, Z. Enhanced stability and catalytic activity on layered perovskite anode for high-performance hybrid direct carbon fuel cells. *ACS Appl. Mater. Interfaces* **2020**, *12*, 12938–12948. <https://doi.org/10.1021/acsami.0c02866>.
106. Ma, M.; Yang, X.; Ren, R.; Xu, C.; Qiao, J.; Sun, W.; Sun, K.; Wang, Z. Honeycombed porous, size matching architecture for high-performance hybrid direct carbon fuel cell anode. *ACS Appl. Mater. Interfaces* **2020**, *12*, 30411–30419. <https://doi.org/10.1021/acsami.0c07350>.
107. Yang, X.; Ma, M.; Xu, C.; Ren, R.; Qiao, J.; Sun, W.; Sun, K.; Wang, Z. Promoting effective electrochemical oxidation of CO by Cu-doping for highly active hybrid direct carbon fuel cell anode. *J. Power Sources* **2022**, *521*, 230966. <https://doi.org/10.1016/j.jpowsour.2021.230966>.
108. Wang, R.; Li, G.; Ma, Y.; Wang, T.; Chen, B.; Wei, T.; Dong, D. A high-performance hybrid direct carbon fuel cell with tandem catalysis in the dendritic channelled anode. *Int. J. Hydrogen Energy* **2023**, *48*, 9797–9804. <https://doi.org/10.1016/j.ijhydene.2022.12.014>.
109. Benamira, M.; Ringuedé, A.; Hildebrandt, L.; Lagergren, C.; Vannier, R.-N.; Cassir, M. Gadolinia-doped ceria mixed with alkali carbonates for SOFC applications: II—An electrochemical insight. *Int. J. Hydrogen Energy* **2012**, *37*, 19371–19379. <https://doi.org/10.1016/j.ijhydene.2011.10.062>.
110. Xu, X.; Zhou, W.; Zhu, Z. Stability of YSZ and SDC in molten carbonate eutectics for hybrid direct carbon fuel cells. *RSC Adv.* **2014**, *4*, 2398–2403. <https://doi.org/10.1039/C3RA46600K>.
111. Ma, M.; Yang, X.; Qiao, J.; Sun, W.; Wang, Z.; Sun, K. Progress and challenges of carbon-fueled solid oxide fuel cells anode. *J. Energy Chem.* **2021**, *56*, 209–222. <https://doi.org/10.1016/j.jechem.2020.08.013>.
112. Kudo, T.; Hisamitsu, Y.; Kihara, K.; Mohamedi, M.; Uchida, I. X-ray diffractometric study of in situ oxidation of Ni in Li/K and Li/Na carbonate eutectic. *J. Power Sources* **2002**, *104*, 272–280. [https://doi.org/10.1016/S0378-7753\(01\)00962-4](https://doi.org/10.1016/S0378-7753(01)00962-4).
113. Cayan, F.N.; Zhi, M.; Pakalapati, S.R.; Celik, I.; Wu, N.; Gemmen, R. Effects of coal syngas impurities on anodes of solid oxide fuel cells. *J. Power Sources* **2008**, *185*, 595–602. <https://doi.org/10.1016/j.jpowsour.2008.06.058>.

114. Lussier, A.; Sofie, S.; Dvorak, J.; Idzerda, Y.U. Mechanism for SOFC anode degradation from hydrogen sulfide exposure. *Int. J. Hydrogen Energy* **2008**, *33*, 3945–3951. <https://doi.org/10.1016/j.ijhydene.2007.11.033>.
115. Antolini, E. Direct propane fuel cells. *Fuel* **2022**, *315*, 123152. <https://doi.org/10.1016/j.fuel.2022.123152>.
116. Sreedhar, I.; Agarwal, B.; Goyal, P.; Singh, S.-A. Recent advances in material and performance aspects of solid oxide fuel cells. *J. Electroanal. Chem.* **2019**, *848*, 113315. <https://doi.org/10.1016/j.jelechem.2019.113315>.
117. Ishihara, T.; Matsuda, H.; Takita, Y. Doped LaGaO<sub>3</sub> perovskite type oxide as a new oxide ionic conductor. *J. Am. Chem. Soc.* **1994**, *116*, 3801–3803. <https://doi.org/10.1021/ja00088a016>.
118. Huang, K.; Wan, J.H.; Goodenough, J.B. Increasing power density of LSGM-based solid oxide fuel cells using new anode materials. *J. Electrochem. Soc.* **2001**, *148*, A788–A794. <https://doi.org/10.1149/1.1378289>.
119. Kawahara, K.; Suda, S.; Suzuki, M.; Kawano, M.; Yoshida, H.; Inagaki, T. Effect of MgO formation in the vicinity of Ni-SDC/LSGM interface on SOFC performance. *Solid State Ion.* **2009**, *180*, 236–240. <https://doi.org/10.1016/j.ssi.2008.11.009>.
120. dos Santos-Gómez, L.; León-Reina, L.; Porras-Vázquez, J.M.; Losilla, E.R.; Marrero-López, D. Chemical stability and compatibility of double perovskite anode materials for SOFCs. *Solid State Ion.* **2013**, *239*, 1–7. <https://doi.org/10.1016/j.ssi.2013.03.005>.
121. Filonova, E.A.; Dmitriev, A.S.; Pikalov, P.S.; Medvedev, D.A.; Pikalova, E.Y. The structural and electrical properties of Sr<sub>2</sub>Ni<sub>0.75</sub>Mg<sub>0.25</sub>MoO<sub>6</sub> and its compatibility with solid state electrolytes. *Solid State Ion.* **2014**, *262*, 365–369. <https://doi.org/10.1016/j.ssi.2013.11.036>.
122. Martinez-Coronado, R.; Alonso, J.A.; Aguader, A.; Fernandez-Diaz, M.T. Optimized energy conversion efficiency in solid-oxide fuel cells implementing SrMo<sub>1-x</sub>Fe<sub>x</sub>O<sub>3-δ</sub> perovskites as anodes. *J. Power Sources* **2012**, *208*, 153–158. <https://doi.org/10.1016/j.jpowsour.2012.02.002>.
123. Jiang, S.P. A comparison of O<sub>2</sub> reduction reactions on porous (La,Sr)MnO<sub>3</sub> and (La,Sr)(Co,Fe)O<sub>3</sub> electrodes. *Solid State Ion.* **2002**, *146*, 1–22. [https://doi.org/10.1016/S0167-2738\(01\)00997-3](https://doi.org/10.1016/S0167-2738(01)00997-3).
124. Sun, C.; Hui, R.; Roller, J. Cathode materials for solid oxide fuel cells: A review. *J. Solid State Electrochem.* **2010**, *14*, 1125–1144. <https://doi.org/10.1007/s10008-009-0932-0>.
125. Jiang, C.; Ma, J.; Arenillas, A.; Irvine, J.T.S. Application of ternary carbonate in hybrid direct coal fuel cells. *ECS Trans.* **2014**, *59*, 281–287. <https://doi.org/10.1149/05901.0281ecst>.
126. Malliaris, A.; Turner, D.T. Influence of particle size on the electrical resistivity of compacted mixtures of polymeric and metallic powders. *J. Appl. Phys.* **1971**, *42*, 614–618. <https://doi.org/10.1063/1.1660071>.
127. Ahn, S.Y.; Eom, S.Y.; Rhie, Y.H.; Sung, Y.M.; Moon, C.E.; Choi, G.M.; Kim, D.J. Application of refuse fuels in a direct carbon fuel cell system. *Energy* **2013**, *51*, 447–456. <https://doi.org/10.1016/j.energy.2012.12.025>.
128. Li, X.; Zhu, Z.H.; De Marco, R.; Bradley, J.; Dicks, A. Evaluation of raw coals as fuels for direct carbon fuel cells. *J. Power Sources* **2010**, *195*, 4051–4058. <https://doi.org/10.1016/j.jpowsour.2010.01.048>.
129. Li, X.; Zhu, Z.H.; De Marco, R.; Dicks, A.; Bradley, J.; Liu, S.M.; Lu, G.Q. Factors that determine the performance of carbon fuels in the direct carbon fuel cell. *Ind. Eng. Chem. Res.* **2008**, *47*, 9670–9677. <https://doi.org/10.1021/ie800891m>.
130. Li, X.; Zhu, Z.; Chen, J.; De Marco, R.; Dicks, A.; Bradley, J.; Lu, G. Surface modification of carbon fuels for direct carbon fuel cells. *J. Power Sources* **2009**, *186*, 1–9. <https://doi.org/10.1016/j.jpowsour.2008.09.070>.
131. Bie, K.; Fu, P.; Liu, Y.; Muhammad, A. Comparative study on the performance of different carbon fuels in a molten carbonate direct carbon fuel cell with a novel anode structure. *J. Power Sources* **2010**, *460*, 228101. <https://doi.org/10.1016/j.jpowsour.2020.228101>.
132. Dudek, M.; Sitarz, M.; Tomczyk, P. Effect of structural properties of carbon-based fuels on efficiency of direct carbon fuel cells. *J. Solid State Electrochem.* **2014**, *18*, 3023–3032. <https://doi.org/10.1007/s10008-014-2442-y>.
133. Qiu, Q.; Zhou, M.; Cai, W.; Zhou, Q.; Zhang, Y.; Wang, W.; Liu, M.; Liu, J. A comparative investigation on direct carbon solid oxide fuel cells operated with fuels of biochar derived from wheat straw, corncob, and bagasse. *Biomass Bioenergy* **2019**, *121*, 56–63. <https://doi.org/10.1016/j.biombioe.2018.12.016>.
134. Cai, W.; Zhou, Q.; Xie, Y.; Liu, J.; Long, G.; Cheng, S.; Liu, M. A direct carbon solid oxide fuel cell operated on a plant derived biofuel with natural catalyst. *Appl. Energy* **2016**, *179*, 1232–124. <https://doi.org/10.1016/j.apenergy.2016.07.068>.
135. Rady, A.C.; Giddey, S.; Kulkarni, A.; Badwal, S.P.S.; Bhattacharya, S.; Ladewig, B.P. Direct carbon fuel cell operation on brown coal. *Appl. Energy* **2014**, *120*, 56–64. <https://doi.org/10.1016/j.apenergy.2014.01.046>.
136. Xu, K.; Dong, J.; Hu, H.; Zhu, X.; Yao, H. Effect of ash components on the performance of solid oxide electrolyte-based carbon fuel cells. *Energy Fuels* **2018**, *32*, 4538–4546. <https://doi.org/10.1021/acs.energyfuels.7b03068>.
137. Liu, G.; Zhang, Y.; Zhou, A.; Wang, J.; Cai, J.; Dang, Y. A Comparative study on the performance of direct carbon solid oxide fuel cell powered with different rank coals. *Energy Fuels* **2021**, *35*, 6835–6844. <https://doi.org/10.1021/acs.energyfuels.1c00051>.
138. Wu, X.; Radovic, L. Catalytic oxidation of carbon/carbon composite materials in the presence of potassium and calcium acetates. *Carbon* **2006**, *43*, 333–344. <https://doi.org/10.1016/j.carbon.2004.09.025>.
139. Dudek, M.; Tomczyk, P. Composite fuel for direct carbon fuel cell. *Catal. Today* **2011**, *176*, 388–292. <https://doi.org/10.1016/j.cattod.2010.11.029>.
140. Wu, Y.; Su, C.; Zhang, C.; Ran, R.; Shao, Z. A new carbon fuel cell with high power output by integrating with in situ catalytic reverse Boudouard reaction. *Electrochem. Commun.* **2009**, *11*, 1265–1268. <https://doi.org/10.1016/j.elecom.2009.04.016>.

141. Tang, Y.; Liu, J. Effect of anode and Boudouard reaction catalysts on the performance of direct carbon solid oxide fuel cells. *Int. J. Hydrogen Energy* **2010**, *35*, 11188–11193. <https://doi.org/10.1016/j.ijhydene.2010.07.068>.
142. Konsolakis, M.; Kaklidis, N.; Kyriakou, V.; Garagounis, I.; Kraia, T.; Arenillas, A.; Menéndez, J.A.; Strandbakke, R.; Marnellos, G.E. The combined impact of carbon type and catalyst-aided gasification process on the performance of a direct carbon solid oxide fuel cell. *Solid State Ion.* **2018**, *317*, 268–275. <https://doi.org/10.1016/j.ssi.2018.01.026>.
143. Skrzypkiewicz, M.; Lubarska-Radziejewska, I.; Jewlski, J. The effect of Fe<sub>2</sub>O<sub>3</sub> catalyst on direct carbon fuel cell performance. *Int. J. Hydrogen Energy* **2015**, *40*, 13090–13098. <https://doi.org/10.1016/j.ijhydene.2015.07.132>.
144. Cai, W.; Liu, J.; Yu, F.; Zhou, Q.; Zhang, Y.; Wang, X.; Liu, M.; Ni, M. A high performance direct carbon solid oxide fuel cell fueled by Ca-loaded activated carbon. *Int. J. Hydrogen Energy* **2017**, *42*, 21167–21176. <https://doi.org/10.1016/j.ijhydene.2017.03.229>.
145. Rady, A.C.; Giddey, S.; Kulkarni, A.; Badwal, S.P.S.; Bhattacharya, S. Catalytic gasification of carbon in a direct carbon fuel cell. *Fuel* **2016**, *180*, 270–277. <https://doi.org/10.1016/j.fuel.2016.04.047>.
146. Cao, T.; Song, P.; Shi, Y.; Cai, N. Carbonate-tin composite liquid anode for solid oxide direct carbon fuel cell. *Int. J. Hydrogen Energy* **2017**, *42*, 6324–6331. <https://doi.org/10.1016/j.ijhydene.2016.11.091>.
147. Li, S.; Jiang, C.; Irvine, J.T.S. Investigation of tin liquid anode on hybrid direct carbon fuel cells. *ECS Trans.* **2019**, *91*, 523–528. <https://doi.org/10.1149/09101.0523ecst>.
148. Tsiapis, E.; Waerenborgh, J.; Kharton, V. Grain-boundary states in solid oxide electrolyte ceramics processed using iron oxide sintering aids: A Mössbauer spectroscopy study. *J. Solid State Electrochem.* **2017**, *21*, 2965–2974. <https://doi.org/10.1007/s10008-017-3622-3>.

**Disclaimer/Publisher’s Note:** The statements, opinions and data contained in all publications are solely those of the individual author(s) and contributor(s) and not of MDPI and/or the editor(s). MDPI and/or the editor(s) disclaim responsibility for any injury to people or property resulting from any ideas, methods, instructions or products referred to in the content.